

1 **Alterations in microbial community composition with increasing $f\text{CO}_2$: a mesocosm study in the**
2 **eastern Baltic Sea**

3

4

5 **Katharine J. Crawford¹, Santiago Alvarez-Fernandez², Kristina D. A. Mojica³, Ulf Riebesell⁴, Corina P.**
6 **D. Brussaard^{1,5}**

7

8 [1]{NIOZ Royal Netherlands Institute for Sea Research, Department of Marine Microbiology and
9 Biogeochemistry and Utrecht University, P.O. Box 59, 1790 AB Den Burg, Texel, The Netherlands}

10

11 [2]{Alfred-Wegener-Institut Helmholtz-Zentrum für Polar- und Meeresforschung, Biologische Anstalt
12 Helgoland, 27498, Helgoland, Germany}

13

14 [3] {Department of Botany and Plant Pathology, Cordley Hall 2082, Oregon State University, Corvallis,
15 Oregon 97331-29052, USA}

16

17 [4]{GEOMAR Helmholtz Centre for Ocean Research Kiel, Biological Oceanography, Düsternbrooker
18 Weg 20, 24105, Kiel, Germany}

19

20 [5]{Aquatic Microbiology, Institute for Biodiversity and Ecosystem Dynamics, University of
21 Amsterdam, P.O. Box 94248, 1090 GE Amsterdam, The Netherlands}

22

23 *Correspondence to:* K. Crawford (kate.crawford@gmail.com) and C. P. D. Brussaard
24 (corina.brussaard@nioz.nl)

25

26

27

28 **Abstract**

29 Ocean acidification, resulting from the uptake of anthropogenic carbon dioxide (CO₂) by the ocean, is
30 considered a major threat to marine ecosystems. Here we examined effects of ocean acidification on
31 microbial community dynamics in the eastern Baltic Sea, during the summer of 2012 when inorganic
32 nitrogen and phosphorus were strongly depleted. Large volume in situ mesocosms were employed to
33 mimic present, future and far future CO₂ scenarios. All six groups of phytoplankton enumerated by
34 flow cytometry (<20 µm cell diameter) showed distinct trends in net growth and abundance with CO₂
35 enrichment. The picoeukaryotic phytoplankton groups Pico-I and II displayed enhanced abundances,
36 whilst Pico-III, *Synechococcus* and the nanoeukaryotic phytoplankton groups were negatively
37 affected by elevated fugacity of CO₂ (*f*CO₂). Specifically, the numerically dominant eukaryote, Pico-I,
38 demonstrated increases in gross growth rate with increasing *f*CO₂ sufficient to double its abundance.
39 Dynamics of the prokaryote community closely followed trends in total algal biomass despite
40 differential effects of *f*CO₂ on algal groups. Similarly, viral abundances corresponded to prokaryotic
41 host population dynamics. Viral lysis and grazing were both important in controlling microbial
42 abundances. Overall our results point to a shift, with increasing *f*CO₂, towards a more regenerative
43 system with production dominated by small picoeukaryotic phytoplankton.

44

45

46 **1 Introduction**

47 Marine phytoplankton are responsible for approximately half of global primary production (Field et
48 al., 1998), with shelf sea communities contributing an average 15-30 % (Kulinski and Pempkowiak,
49 2011). Since the industrial revolution atmospheric carbon dioxide (CO₂) concentrations have
50 increased by nearly 40 % due to anthropogenic emissions, primarily caused by the burning of fossil
51 fuels and deforestation (Doney et al., 2009). Atmospheric CO₂ dissolves in the oceans where it forms
52 carbonic acid which reduces seawater pH, a process commonly termed, ocean acidification (OA).

53 Currently, along with warming sea surface temperatures and changing light and nutrient conditions,
54 marine ecosystems face unprecedented decreases in ocean pH (Doney et al., 2009; Gruber, 2011).
55 Ocean acidification is considered one of the greatest current threats to marine ecosystems (Turley
56 and Boot, 2010) and has been shown to alter phytoplankton primary production with the direction
57 and magnitude of the responses dependent on community composition (eg. Hein and Sand-Jensen,
58 1997; Tortell et al., 2002; Leonardos and Geider, 2005; Engel et al., 2007; Feng et al., 2009; Eberlein
59 et al., 2017). Certain cyanobacteria, including diazotrophs, demonstrate stimulated growth under
60 conditions of elevated CO₂ (Qiu and Gao, 2002; Barcelos e Ramos et al., 2007; Hutchins, 2007;
61 Dutkiewicz et al., 2015). However, no consistent trends have been found for *Synechococcus* (Schulz
62 et al., 2017 and references therein). The responses of diatoms and coccolithophores also appear
63 more variable (Dutkiewicz et al., 2015 and references therein), although coccolithophore calcification
64 seems generally negatively impacted (Meyer and Riebesell, 2015; Riebesell et al., 2017). OA has also
65 been reported to increase the abundances of small-sized photoautotrophic eukaryotes in mesocosm
66 experiments (Engel et al., 2007; Meakin and Wyman, 2011; Brussaard et al., 2013; Schulz et al.,
67 2017).

68 Recently, data regarding the effects of OA on taxa-specific phytoplankton growth rates were
69 incorporated into a global ecosystem model. The results emphasized that elevated CO₂
70 concentrations can cause changes in community structure by altering the competitive fitness, and
71 thus competition between phytoplankton groups (Dutkiewicz et al., 2015). Moreover, OA was found
72 to have a greater impact on phytoplankton community size structure, function and biomass than
73 either warming or reduced nutrient supply (Dutkiewicz et al., 2015). Many OA studies have been
74 conducted using single-species under controlled laboratory conditions and therefore cannot account
75 for intrinsic community interactions that occur under natural conditions. Alternatively, larger-volume
76 mesocosm experiments allow for OA manipulation of natural communities and as such, are more
77 likely to capture and quantify the overall response of the natural ecosystems. To date, the majority of
78 these experiments started under replete nutrient conditions or received nutrient additions (Paul et

79 al., 2015 and references therein). Thus, little data is available for oligotrophic conditions, which are
80 present in ~75% of the world's oceans (Corno et al., 2007).

81 Whilst environmental factors such as temperature, light, nutrient and CO₂ concentrations regulate
82 gross primary production, loss factors determine the fate of this photosynthetically fixed carbon.
83 Grazing, sinking and viral lysis affect the cycling of elements in different manners, i.e. transferred to
84 higher trophic levels through grazing, carbon sequestration in deep waters and sediments, and
85 cellular content release by viral lysis (Wilhelm and Suttle, 1999; Brussaard et al., 2005). Released
86 detrital and dissolved organic matter (DOM) is quickly utilized by heterotrophic bacteria, thereby
87 stimulating activity within the microbial loop (Brussaard et al., 2008; Lønborg et al., 2013; Sheik et al.,
88 2014; Middelboe and Lyck, 2002). Consequently, bacteria may be affected indirectly by OA through
89 changes in the quality and/or quantity of DOM (Weinbauer et al., 2011). Viral lysis has been found to
90 be as important as microzooplankton grazing to the mortality of natural bacterio- and phytoplankton
91 (Weinbauer, 2004; Baudoux et al., 2006; Evans and Brussaard, 2012; Mojica et al., 2016). Thus far,
92 most studies examining the effects of OA on microzooplankton abundance and/or grazing have
93 found little or no direct effect (Suffrian et al., 2008; Rose et al., 2009; Aberle et al., 2013; Brussaard et
94 al., 2013; Niehoff et al., 2013). To our knowledge, no viral lysis rates have been reported for natural
95 phytoplankton communities under conditions of OA. A few studies have inferred rates based on
96 changes in viral abundances under enhanced CO₂, but the results are inconsistent (Larsen et al.,
97 2008; Brussaard et al., 2013). Therefore, the effect of OA on the relative share of these key loss
98 processes is still understudied for most ecosystems.

99 Here we report on the temporal dynamics of microbes (phytoplankton, prokaryotes and viruses)
100 under the influence of enhanced CO₂ concentrations in the low-salinity (around 5.7) Baltic Sea. Using
101 large mesocosms with in situ light and temperature conditions, the pelagic ecosystem was exposed
102 to a range of increasing CO₂ concentrations from ambient to future and far future concentrations.
103 The study was performed during the summer in the Baltic Sea near Tvärminne when conditions were
104 oligotrophic. Our data show, that over the 43 day long experiment, enhanced CO₂ concentrations

105 elicited distinct shifts in the microbial community, most notably an increase in the net growth of
106 small picoeukaryotic phytoplankton.

107

108 **2 Materials and Methods**

109 **2.1 Study site and experimental set-up**

110 The present study was conducted in the Tvärminne Storfjärden (59° 51.5' N, 23° 15.5' E) between 14
111 June and 7 August, 2012. Nine mesocosms, each enclosing ~55 m³ of water, were moored in a square
112 arrangement at a site with a water depth of approximately 30 m. The mesocosms consisted of open
113 ended polyurethane bags 2 m in diameter and 18.5 m in length mounted onto floating frames
114 covered at each end with a 3 mm mesh. Initially, the mesocosms were kept open for 5 days to allow
115 for rinsing and water exchange while excluding large organisms from entering with the 3 mm mesh.
116 During this time, the bags were positioned such that the tops were submerged 0.5 m below the
117 water surface and the bottoms reached down to 17 m depth in the water column. Photosynthetically
118 active radiation (PAR) transparent plastic hoods (open on the side) prevented rain and bird droppings
119 from entering the mesocosms, which would affect salinity and nutrients, respectively. Five days
120 before the CO₂ treatment was to begin, the water column of the mesocosms was isolated from the
121 influence of the surrounding water. To do so, the 3 mm mesh was removed and sediment traps (2 m
122 long) were attached to close off the bottom of the mesocosms. The top ends of the bags were raised
123 and secured to the frame 1.5 m above the water surface to prevent water entering via wave action.
124 The mesocosms were then bubbled with compressed air for 3.5 min, to remove salinity gradients and
125 ensure that the water body was fully homogeneous.

126 The present manuscript includes results from six of the original mesocosms, due to the unfortunate
127 loss of three mesocosms which were compromised by leakage. The mean fugacity of CO₂ (*f*CO₂)
128 during the experiment, i.e. days 1-43, for the individual mesocosms were as follows: M1, 365 µatm;
129 M3, 1007 µatm; M5, 368 µatm; M6, 821 µatm; M7, 497 µatm; M8, 1231 µatm (Table 1). The gradient
130 of non-replicated *f*CO₂ of the present study (as opposed to a smaller number of replicated treatment

131 levels) was selected as a balance between the necessary, but manageable, number of mesocosms
132 and minimizing the impact of the high potential for loss of mesocosms to successfully address the
133 underlying questions of the study (Schulz et al., 2013). Moreover, it maximizes the potential of
134 identifying a threshold $f\text{CO}_2$ level concentration, if present (by allowing for a larger number of
135 treatment levels). Carbon dioxide manipulation was carried out in four steps and took place between
136 days 0 to 4 until the target $f\text{CO}_2$ was reached. Initial $f\text{CO}_2$ was 240 μatm . For $f\text{CO}_2$ manipulations, 50
137 μm filtered natural seawater was saturated with CO_2 and then injected evenly throughout the depth
138 of the mesocosms as described by Riebesell et al. (2013). Two mesocosms functioned as controls and
139 were treated in a similar manner using only filtered seawater. On day 15, a supplementary $f\text{CO}_2$
140 addition was made to the top 7 m of mesocosms numbered 3, 6, and 8 to replace CO_2 lost due to
141 outgassing (Paul et al., 2015; Spilling et al., 2016). Throughout this study we refer to $f\text{CO}_2$ which
142 accounts for the non-ideal behavior of CO_2 gas and is considered the standard measurement
143 required for gas exchange (Pfeil et al., 2012).

144 Initial nutrient concentrations were 0.05 $\mu\text{mol L}^{-1}$, 0.15 $\mu\text{mol L}^{-1}$, 6.2 $\mu\text{mol L}^{-1}$ and 0.2 $\mu\text{mol L}^{-1}$ for
145 nitrate, phosphate, silicate and ammonium, respectively. Nutrient concentrations remained low for
146 the duration of the experiment (Paul et al., 2015, this issue) and no nutrients were added. Salinity
147 was relatively constant around 5.7. Temperature was more variable; on average temperature within
148 the mesocosms (0-17 m) increased from ~ 8 $^{\circ}\text{C}$ to a maximum on day 15 of ~ 15 $^{\circ}\text{C}$ and then decreased
149 again to ~ 8 $^{\circ}\text{C}$ by day 30. For further details of the experimental set-up, carbonate chemistry
150 dynamics and nutrient concentrations throughout the experiment we refer to the general overview
151 paper by Paul et al. (2015).

152 Collective sampling was performed every morning using depth integrated water samplers (IWS,
153 HYDRO-BIOS, Kiel). These sampling devices were gently lowered through the water column collecting
154 ~ 5 L of water gradually between 0-10 m (top) or 0-17 m (whole water column). Water was collected
155 from all mesocosms and the surrounding water. Subsamples were obtained for enumeration of
156 phytoplankton, prokaryotes and viruses. Samples for viral lysis and grazing experiments were taken

157 from 5 m depth using a gentle vacuum-driven pump system. Samples were protected against sunlight
158 and warming by thick black plastic bags containing wet ice. Samples were processed at in situ
159 temperature (representative of 5 m depth) under dim light and handled using nitrile gloves. As viral
160 lysis and grazing rates were determined from samples taken from 5 m depth, samples for microbial
161 abundances reported here were taken from the top 10 m integrated samples.

162 The experimental period has been divided into four phases based on major physical and biological
163 changes (Paul et al., 2015): Phase 0 before CO₂ addition (days -5 to 0), Phase I (days 1-16), Phase II
164 (days 17-30) and Phase III (days 31-43). Throughout this manuscript the data are presented using
165 three colors (blue, grey and red), representing low (mesocosms M1 and M5) intermediate (M6 and
166 M7) and high (M3 and M8) *f*CO₂ levels (Table 1).

167

168 **2.2 Microbial abundances**

169 Microbes were enumerated using a Becton Dickinson FACSCalibur flow cytometer (FCM) equipped
170 with a 488 nm argon laser. The samples were stored on wet ice and in the dark until counting. The
171 photoautotrophic cells (<20 µm) were counted directly using fresh seawater and were discriminated
172 by their autofluorescent pigments. Six phytoplankton clusters were differentiated based on the
173 bivariate plots of either chlorophyll (red autofluorescence) or phycoerythrin (orange
174 autofluorescence, for *Synechococcus* and Pico-III) against side scatter. The size of the different
175 phytoplankton clusters was determined by gentle filtration through 25 mm diameter polycarbonate
176 filters (Whatman) with a range of pore sizes (12, 10, 8, 5, 3, 2, 1, and 0.8 µm) according to Veldhuis
177 and Kraay (2004). Average cell sizes for the different phytoplankton groups were 1, 1, 3, 2.9, 5.2, and
178 8.8 µm diameter for the prokaryotic cyanobacteria *Synechococcus* spp. (SYN), picoeukaryotic
179 phytoplankton I, II and III (Pico-I-III), and nanoeukaryotic phytoplankton I, and II (Nano-I, II),
180 respectively. Pico-III was discriminated from Pico-II (comparable average cell size) by a higher orange
181 autofluorescence signature, potentially representing small-sized cryptophytes (Klaveness, 1989);
182 alternatively large single cells or microcolonies of *Synechococcus* (Haverkamp et al., 2009). The

183 cyanobacterial species *Prochlorococcus* spp. were not observed during this experiment. Counts were
184 converted to cellular carbon by assuming a spherical shape equivalent to the average cell diameters
185 determined from size fractionations and applying conversion factors of 237 fg C μm^{-3} (Worden et al.,
186 2004) and 196.5 fg C μm^{-3} (Garrison et al., 2000) for pico- and nano-sized plankton, respectively.
187 Microbial net growth and loss rates were derived from exponential regressions of changes in the cell
188 abundances over time.

189 Abundances of prokaryotes and viruses were determined from 0.5 % glutaraldehyde fixed, flash
190 frozen (-80 °C) samples according to Marie et al. (1999) and Brussaard (2004), respectively. The
191 prokaryotes include heterotrophic bacteria, archaea and unicellular cyanobacteria, the latter
192 accounting for maximal 10 % of the total abundance in our samples, as indicated by their
193 autofluorescence. Briefly, thawed samples were diluted with sterile autoclaved Tris-EDTA buffer (10
194 mM Tris-HCl and 1 mM EDTA, pH 8.2; Mojica et al., 2014) and stained with the green fluorescent
195 nucleic acid-specific dye SYBR-Green I (Invitrogen Inc.) to a final concentration of the commercial
196 stock of 1.0×10^{-4} (for prokaryotes) or 0.5×10^{-4} (for viruses). Virus samples were stained at 80 °C for
197 10 min and then allowed to cool for 5 min at room temperature in the dark. Prokaryotes were
198 stained for 15 min at room temperature in the dark (Brussaard, 2004). Prokaryotes and viruses were
199 discriminated in bivariate scatter plots of green fluorescence versus side scatter. Final counts were
200 corrected for blanks prepared and analyzed in a similar manner as the samples. Two groups of
201 prokaryotes were identified by their stained nucleic acid fluorescence, referred here on as low (LNA)
202 and high (HNA) fluorescence prokaryotes.

203

204 **2.3 Viral lysis and grazing**

205 Microzooplankton grazing and viral lysis of phytoplankton was determined using the modified
206 dilution assay, based on reducing grazing and viral lysis mortality pressure in a serial manner allowing
207 for increased phytoplankton growth (over the incubation period) with dilution (Mojica et al., 2016).
208 Briefly, two dilution series were created in clear 1.2 L polycarbonate bottles by gently mixing 200 μm

209 sieved whole seawater with either 0.45 μm filtered seawater (i.e. microzooplankton grazers
210 removed) or 30 KDa filtered seawater (i.e. grazers and viruses removed) to final dilutions of 20, 40,
211 70 and 100 %. The 0.45 μm filtrate was produced by gravity filtration of 200 μm mesh sieved
212 seawater through a 0.45 μm Sartopore capsule filter. The 30 KDa ultrafiltrate was produced by
213 tangential flow filtration of 200 μm pre-sieved seawater using a 30 kDa Vivaflow 200 PES membrane
214 tangential flow cartridge (Vivascience). All treatments were performed in triplicate. Bottles were
215 suspended next to the mesocosms in small cages at 5 m depth for 24 hours. Subsamples were taken
216 at 0 and 24 h, and phytoplankton abundances of the grazing series (0.45 μm diluent) were
217 enumerated by flow cytometry. Due to time constraint, the majority of the samples of the 30 kDa
218 series were fixed with 1 % (final concentration) formaldehyde : hexamine solution (18 % v/v : 10 %
219 w/v), for 30 min at 4 °C, flash frozen in liquid nitrogen and stored at -80 °C until flow cytometry
220 analysis in the home laboratory. Fixation had no significant effect (student's t-tests, p-value >0.05) as
221 tested periodically against fresh samples. The modified dilution assay was only run for Mesocosms 1
222 (low $f\text{CO}_2$) and 3 (high $f\text{CO}_2$) due to the logistics of handling times. Experiments were performed until
223 day 31. Grazing rates and the combined rate of grazing and viral lysis were estimated from the slope
224 of a regression of phytoplankton apparent growth versus dilution of the 0.45 μm and 30 kDa series,
225 respectively. A significant difference between the two regression coefficients (as tested by analysis of
226 covariance) indicated a significant viral lysis rate. Phytoplankton gross growth rate, in the absence of
227 grazing and viral lysis, was derived from the y-intercept of the 30 kDa series regression. Similarly,
228 significant differences between mesocosms M1 and M3 (low and high $f\text{CO}_2$) were determined
229 through analysis of covariance of the dilution series for the two mesocosms. A significance threshold
230 of 0.05 was used and significance is denoted throughout the manuscript by an asterisk (*).
231 Occasionally, the regression of apparent growth rate versus fraction of natural water resulted in a
232 positive slope (thus no reduction in mortality with dilution). In addition, very low phytoplankton
233 abundances can also prohibit statistical significance of results. Under such conditions dilution

234 experiments were deemed unsuccessful (see for limitations of the modified dilution method,
235 Baudoux et al., 2006; Kimmance and Brussaard, 2010; Stoecker et al., 2015).

236 Viral lysis of prokaryotes was determined according to the viral production assay (Wilhelm et al.,
237 2002; Winget et al., 2005). After reduction of the natural virus concentration, new virus production
238 by the natural bacterial community is sampled and tracked over time (24 h). Briefly, free viruses were
239 reduced from a 300 ml sample of whole water by re-circulation over a 0.2 μm pore size polyether
240 sulfone membrane (PES) tangential flow filter (Vivaflow 50, Vivascience) at a filtrate expulsion rate of
241 40 ml min^{-1} . The concentrated sample was then reconstituted to the original volume using virus-free
242 seawater. This process was repeated a total of three times to gradually wash away viruses. After the
243 final reconstitution, 50 ml aliquots were distributed into six polycarbonate tubes. Mitomycin C
244 (Sigma-Aldrich) (final concentration, 1 $\mu\text{g ml}^{-1}$, maintained at 4 $^{\circ}\text{C}$), which induces lysogenic bacteria
245 (Weinbauer and Suttle, 1996) was added to a second series of triplicate samples for each mesocosm.
246 A third series of incubations with 0.2 μm filtered samples was used as a control for viral loss (e.g.
247 viruses adhering to the tube walls) and showed no significant loss of free viruses during the
248 incubations. At the start of the experiment, 1 ml subsamples were immediately removed from each
249 tube and fixed as previously described for viral and bacterial abundance. The samples were dark
250 incubated at in situ temperature and 1 ml subsamples were taken at 3 h, 6 h, 9 h, 12 h and 24 h.
251 Virus production was determined from linear regression of viral abundance over time. Viral
252 production due to induction of lysogeny was calculated as the difference between production in the
253 unamended samples and production of samples to which mitomycin C was added. Although
254 mortality experiments were initially planned to be employed for mesocosms 1, 2, and 3 representing
255 low, mid and high $f\text{CO}_2$ conditions, mesocosm 2 was compromised due to leakage. Additionally, due
256 to logistical reasons assays were only performed until day 21.

257 To determine grazing rates on prokaryotes, fluorescently labeled bacteria (FLBs) were prepared from
258 enriched natural bacterial assemblages (originating from the North Sea) labeled with 5-([4,6-
259 Dichlorotriazin-2-yl]amino) fluorescein (DTAF, 36565 Sigma-Aldrich 40 $\mu\text{g ml}^{-1}$) according to Sherr et

260 al. (1993). Frozen ampoules of FLB (1-5 % of total bacterial abundance) were added to triplicate 1 L
261 incubation bottles containing whole water gently passed through 200 μm mesh. Twenty ml samples
262 were taken immediately after addition (0 h) and the headspace was removed by gently squeezing air
263 from the bottle. The 1 L bottles were incubated on a slow turning wheel (1 rpm) at in situ light and
264 temperature conditions (representative of 5 m depth) for 24 h. Sampling was repeated after 24 h. All
265 samples were fixed to a 1 % final concentration of glutaraldehyde (0.2 μm filtered; 25 % EM-grade),
266 stained (in the dark for 30 min at 4 $^{\circ}\text{C}$) with 4',6-Diamidino-2-Phenylindole, Dihydrochloride (DAPI)
267 solution (0.2 μm filtered; Acrodisc [®]25 mm Syringe filters, PALL Life Sciences; 2 $\mu\text{g ml}^{-1}$ final
268 concentration; Sherr et al., 1993) and filtered onto 25 mm, 0.2 μm black polycarbonate filters (GE
269 Healthcare life sciences). Filters were then mounted on microscopic slides and stored at -20 $^{\circ}\text{C}$ until
270 analysis. FLBs present on a $\sim 0.75 \text{ mm}^2$ area were counted using a Zeiss Axioplan 2 microscope.
271 Grazing ($\mu \text{ d}^{-1}$) was measured according to $N_{T24} = N_{T0} * e^{-\mu t}$, where N_{T24} and N_{T0} are the number of FLBs
272 present at 24 h and 0 h, respectively.

273

274 **2.4 Statistics**

275 Non-metric multidimensional scaling (NMDS) was used to follow microbial community development
276 in each mesocosm over the experimental period. NMDS is an ordination technique which represents
277 the dissimilarities obtained from an abundance data matrix in a 2-dimensional space (Legendre and
278 Legendre, 1998). In this case, the data matrix was comprised of abundance data for each
279 phytoplankton group in each mesocosm for every day of sampling. The treatment effect was
280 assessed by analysis of similarity (ANOSIM; Clarke, 1993) and inspection of the NMDS biplot. ANOSIM
281 compares the mean of ranked dissimilarities of mesocosms between $f\text{CO}_2$ treatments (low: 1, 5, 7;
282 high: 6, 3, 8) to the mean of ranked dissimilarities within treatments per phase. The NMDS plots
283 allowed divergence periods in the development and community composition between treatments to
284 be visually assessed (period 1 from day 3-13 and period 2 from days 16-24). Net growth rates of each
285 of the different microbial groups were calculated for these identified divergence periods.

286 Relationships between net growth rates and peak cell abundances with $f\text{CO}_2$ were evaluated by
287 linear regression against the average $f\text{CO}_2$ per mesocosm during each period or peak day. A
288 generalized linear model was used to test the relationship between prokaryote abundance and
289 carbon biomass with an ARMA correlation structure of order 3 to account for temporal
290 autocorrelation. The model fulfilled all assumptions such as homoscedasticity and avoiding
291 autocorrelation of the residuals (Zuur et al., 2007). A significance threshold of $p \leq 0.05$ was used and
292 significance is denoted by an asterisk (*). All analyses were performed using the statistical software
293 program R, using packages nlme (Pinheiro et al., 2017) and vegan (Oksanen et al., 2017) (R core
294 Team, 2017). Where average of low and high mesocosm abundance data are reported, values
295 represent the average of mesocosms 1, 5, 7 (mean $f\text{CO}_2$ 365-497 μatm) and 6, 3, 8 (821-1231 μatm),
296 respectively.

297

298 **3 Results**

299 **3.1 Total phytoplankton dynamics in response to CO_2 enrichment**

300 During Phase 0, low variability in phytoplankton abundances in the different mesocosms ($1.5 \pm 0.05 \times$
301 10^5 ml^{-1}) indicated good replicability of initial conditions prior to CO_2 manipulation (Fig. 1). This was
302 further supported by the high similarity between microbial communities in the different mesocosms
303 as indicated by the tight clustering of points in the NMDS plot during this period (Fig. 2). During
304 Phase 0, the phytoplankton community ($<20 \mu\text{m}$) was dominated by pico-sized autotrophs, with the
305 prokaryotic cyanobacteria *Synechococcus* (SYN) and Pico-I accounting for 69 % and 27 % of total
306 phytoplankton abundance, respectively. After CO_2 addition, there were two primary peaks in
307 phytoplankton, which occurred on day 4 in Phase I and day 24 in Phase II (Fig. 1a). The phytoplankton
308 community became significantly different over time in the different treatments (ANOSIM, $p=0.01$,
309 Fig. 2). Two periods were identified based on their divergence (Fig.2), the first (NMDS-based period
310 1) followed the initial peak in abundance (days 3-13) with highest abundances occurring in the
311 elevated CO_2 mesocosms (Fig. 1a). During the second period (NMDS-based period 2, days 16-24),

312 abundances were higher in the low $f\text{CO}_2$ mesocosms (Fig. 1a). In general the NMDS plot shows that
313 throughout the experiment, mesocosm M1 followed the same basic trajectory as mesocosms M5 and
314 M7, whilst mesocosm M3 followed M6 and M8 (Fig. 2). Thus, the two mesocosms (representing high
315 and low $f\text{CO}_2$ treatments) deviated from each other during Phase I and were clearly separated during
316 Phases II and III (Fig. 2).

317 Phytoplankton abundances in the surrounding water started to differ from the mesocosms during
318 Phase 0 (on average 44 % lower) which was primarily due to lower abundances of SYN. This effect
319 was seen from day -1, prior to CO_2 addition but following bubbling with compressed air (day -5). On
320 day 15, a deep mixing event occurred as a result of storm conditions (with consequent alterations in
321 temperature and salinity) and as a result phytoplankton abundances in the surrounding open water
322 diverged more strongly from the mesocosms but remained similar in their dynamics (Fig. 3).
323 Microbial abundances in the 0-17 m samples were slightly lower but showed very similar dynamics to
324 those in the 0-10 m samples (Fig. S1).

325

326 **3.1.1 *Synechococcus***

327 The prokaryotic cyanobacteria *Synechococcus* (SYN) accounted for the majority of total abundance,
328 i.e. 74 % averaged across all mesocosms over the experimental period. Abundances of SYN showed
329 distinct variability between the different CO_2 treatments, starting on day 7, with the low CO_2
330 mesocosms exhibiting nearly 20 % lower abundances between days 11-15 as compared to high $f\text{CO}_2$
331 mesocosms (Fig. 3a). SYN net growth rates during days 3-13 (NMDS-based period 1) were positively
332 correlated with CO_2 ($p=0.10$, $R^2=0.53$; Table 2, Fig. S2a). One explanation for higher net growth rates
333 at elevated CO_2 could be the significantly ($p<0.05$) higher grazing rate in the low $f\text{CO}_2$ mesocosm M1
334 (0.56 d^{-1}) compared to the high $f\text{CO}_2$ M3 (0.27 d^{-1}) as measured on day 10 (Fig. 4a). After day 16, SYN
335 abundances increased in all mesocosms and during this period (days 16-24) net growth rates had a
336 significant negative correlation to $f\text{CO}_2$ ($p=0.05$, $R^2= 0.63$; Figs. 3a, Table 2 and Fig. S3a).
337 Consequently, the net increase in SYN abundances during this period was on average 20 % higher at

338 low $f\text{CO}_2$ compared to high $f\text{CO}_2$. This corresponded to higher total loss rates in high $f\text{CO}_2$ treatments
339 measured on day 17 (0.33 vs 0.17 d^{-1} for M3 and M1, respectively; Fig. 4a). The higher net growth
340 most likely led to the peak in SYN abundance observed on day 24 (max. $4.7 \times 10^5 \text{ ml}^{-1}$), which was
341 negatively correlated with $f\text{CO}_2$ ($p=0.01$, $R^2=0.80$; Table 3, Fig. S4a). After this period (days 24-28),
342 SYN abundances declined at comparable rates in the different mesocosms, irrespective of $f\text{CO}_2$ (Fig.
343 3a). Abundances in the low $f\text{CO}_2$ mesocosms remained higher into Phase III (Fig. 3a). SYN abundances
344 in the surrounding water were generally lower than in the mesocosms, with the exception of days
345 17-21.

346

347 **3.1.2 Picoeukaryotes**

348 In contrast to the prokaryotic photoautotrophs, the eukaryotic phytoplankton community showed a
349 strong positive response to elevated $f\text{CO}_2$ (Fig. 1b). Pico-I was the numerically dominant group of
350 eukaryotic phytoplankton, accounting for an average 21-26 % of total phytoplankton abundances.
351 Net growth rates leading up to the first peak in abundance (from day 1 to 5) had a strong positive
352 correlation with $f\text{CO}_2$ ($p<0.01$, $R^2=0.90$; Fig. 3b, Table 3, Fig. S5a). Accordingly, the peak on day 5
353 (max. $1.1 \times 10^5 \text{ ml}^{-1}$; Fig. 3b) was also correlated positively with $f\text{CO}_2$ ($p=0.01$, $R^2=0.81$; Table 3, Fig.
354 S4b). During Phase I, from days 3-13 (i.e. NMDS-based period 1), net growth rates of Pico-I remained
355 positively correlated to CO_2 concentration ($p=0.01$, $R^2=0.80$; Table 2, Fig. S2b). However, during this
356 period there was also a decline in abundance (days 5-9; $p<0.01$, $R^2=0.89$; Table 3, Fig. S5b) with 23 %
357 more cells lost in the low $f\text{CO}_2$ mesocosms. Accordingly, following this period, gross growth rate was
358 significantly higher in the high $f\text{CO}_2$ mesocosm M3 as compared to the low $f\text{CO}_2$ mesocosm M1 (day
359 10, $p<0.05$; Fig. 4b). Pico-I abundances in the surrounding open water started to deviate from the
360 mesocosms after day 10, and were on average around half that of the low $f\text{CO}_2$ mesocosms (Fig. 3b).
361 Following a brief increase (occurring between days 11-13) correlated to $f\text{CO}_2$ ($p<0.01$, $R^2=0.94$; Table
362 3, Fig. S4c), abundances declined sharply between days 13-16 (Fig. 3b), coinciding with a significantly
363 higher total mortality rate in the high $f\text{CO}_2$ mesocosm M3 (day 13; Fig. 4b). Viral lysis was a

364 substantial loss factor relative to grazing, for this group, comprising an average 45 % and 70 % of
365 total losses in M1 and M3, respectively (Table S1). During NMDS-based period 2, net growth rates of
366 Pico-I were significantly higher at high $f\text{CO}_2$ ($p=0.05$, $R^2=0.64$; Table 2, Fig S3b). By day 21,
367 abundances in the high $f\text{CO}_2$ mesocosms were (on average) ~2-fold higher than at low $f\text{CO}_2$
368 (maximum abundances $8.7 \times 10^4 \text{ ml}^{-1}$ and $5.9 \times 10^4 \text{ ml}^{-1}$ for high and low $f\text{CO}_2$ mesocosms; $p=0.01$,
369 $R^2=0.84$; Table 3, Fig. S4d). Standing stock of Pico-I remained high in the elevated $f\text{CO}_2$ mesocosms
370 for the remainder of the experiment (7.9×10^4 vs $4.3 \times 10^4 \text{ ml}^{-1}$ on average for high and low $f\text{CO}_2$
371 mesocosms, respectively; Fig. 3b). Additionally, gross growth rates during this final period were
372 relatively low (0.14 and 0.16 d^{-1} in M1 and M3, respectively) and comparable to total loss rates
373 (averaging 0.13 and 0.10 d^{-1} over days 25-31, for M1 and M3, respectively; Fig. 4b).

374 Another pico-eukaryote group, Pico-II, slowly increased in abundance until day 13, when it increased
375 more rapidly (Fig. 3c). Gross growth rates measured during Phase I were high (0.69 and 0.72 d^{-1} on
376 average in the low and high $f\text{CO}_2$ mesocosms M1 and M3, respectively; Fig. 4c), and comparable to
377 loss processes (0.46 and 0.58 d^{-1}), indicative of a relatively high turnover rate of production. Overall
378 net growth rates during days 3-13 (NMDS-based period 1) did not correlate to CO_2 ($p=0.52$, $R^2=0.11$;
379 Table 2, Fig. S2c). However, during periods of rapid increases in net growth, abundances were
380 positively correlated to CO_2 concentration (days 12-17; $p=0.01$, $R^2=0.82$; Table 3, Fig. S5c).
381 Accordingly, the peak in abundances of Pico-II on day 17 displayed a distinct positive correlation with
382 $f\text{CO}_2$ ($p<0.01$, $R^2=0.93$; Table 3, Fig. S4e), with maximum abundances of $4.6 \times 10^3 \text{ ml}^{-1}$ and 3.4×10^3
383 ml^{-1} for the high and low $f\text{CO}_2$ mesocosms, respectively (Fig. 3c). In M8 (the highest $f\text{CO}_2$ mesocosm),
384 abundances increased for an extra day with the peak occurring on day 18, resulting in an average 23
385 % higher abundances. During the decline of the Pico-II peak (days 16-24), net growth rates were
386 negatively correlated with $f\text{CO}_2$ ($p=0.10$, $R^2=0.52$; Table 2, Fig S3c). Moreover, the rate of decline was
387 faster for the high $f\text{CO}_2$ mesocosms during days 18-21 ($p<0.01$, $R^2=0.85$). The Pico-II abundances in
388 the surrounding water were comparable to the mesocosms during Phases 0 and I, lower during
389 Phase II and higher during Phase III (Fig. 3c).

390 Pico-III exhibited a short initial increase in abundances in the low $f\text{CO}_2$ treatments, resulting in nearly
391 2-fold higher abundances at low $f\text{CO}_2$ by day 3 compared to the high $f\text{CO}_2$ treatment (Fig. 3d). After
392 this initial period, net growth rates of this group had a significant positive correlation with $f\text{CO}_2$ (days
393 3-13; $p=0.04$, $R^2=0.67$; Table 2, Fig. S2d). In general, during Phase I gross growth ($p<0.01$, days 1, 3,
394 10; Fig. 4d) and total mortality ($p<0.05$, days 1, 6, 10; Fig. 4d) were significantly higher in the low $f\text{CO}_2$
395 mesocosm M1, as compared to the high $f\text{CO}_2$ mesocosm M3 resulting in low net growth rates. During
396 Phase II (days 16-24, NMDS-based period 2) the opposite occurred; i.e. net growth rates were
397 negatively correlated with $f\text{CO}_2$ ($p<0.01$, $R^2=0.86$; Table 2, Fig S.3d). Maximum Pico-III abundances
398 (day 24: 4.2×10^3 and $8.3 \times 10^3 \text{ ml}^{-1}$ for high and low $f\text{CO}_2$) had a strong negative correlation with $f\text{CO}_2$
399 ($p<0.01$, $R^2=0.91$; Table 3, Fig. S4f). Pico-III abundances remained noticeably higher in the low $f\text{CO}_2$
400 mesocosms during Phases II and III (on average 80 %; Fig. 3d). Unfortunately, almost half of the
401 mortality assays in this second half of the experiment failed (see Materials and Methods), but the
402 successful assays suggest that losses were minor ($<0.15 \text{ d}^{-1}$; Fig. 4d) and primarily due to grazing, as
403 no significant viral lysis was detected (Table S1).

404

405 3.1.3 Nanoeukaryotes

406 Nano-I showed maximum abundances ($4.3 \pm 0.4 \times 10^2 \text{ ml}^{-1}$) on day 6 (except M1 which peaked on day
407 5), independent of $f\text{CO}_2$ ($p=0.23$, $R^2=0.33$; Fig. 3e). There was, however, a negative correlation of net
408 growth rate with $f\text{CO}_2$ during days 3-13 (NMDS-based period 1; $p=0.01$, $R^2=0.79$; Table 2, Fig. S2e). A
409 second major peak in abundance of Nano-I occurred on day 17, with markedly higher numbers in the
410 low $f\text{CO}_2$ mesocosms ($4.1 \times 10^2 \text{ ml}^{-1}$ as compared to $2.4 \times 10^2 \text{ ml}^{-1}$ in high $f\text{CO}_2$ mesocosms; $p=0.04$,
411 $R^2=0.67$; Fig. 3e, Table 3 and Fig. S4g). Total loss rates in the high $f\text{CO}_2$ mesocosm M3 on days 6 and
412 10 were 2.3-fold higher compared to the low $f\text{CO}_2$ mesocosm M1 (Fig. 4e), which may help to
413 explain this discrepancy in total abundance between low and high $f\text{CO}_2$ mesocosms. Viral lysis made
414 up to 98 % of total losses in the high $f\text{CO}_2$ mesocosm M3 during this period, whilst in M1 viral lysis
415 was only detected on day 13 (Table S1). Peak abundances (around $5.0 \times 10^2 \text{ ml}^{-1}$) were much lower

416 compared to those in the surrounding waters (max $\sim 2.4 \times 10^3 \text{ ml}^{-1}$; Figs. 3e and S6a). During Phase II,
417 Nano-I abundances in the surrounding waters displayed rather erratic dynamics compared to those
418 of the mesocosms, but converged during certain periods (e.g. days 19-22). No significant relationship
419 was found between net loss rates and $f\text{CO}_2$ for the second NMDS-based period ($p=0.26$, $R^2=0.30$;
420 Table 2, Fig S.3e). At the end of Phase II, abundances were similar in all mesocosms but diverged
421 again during Phase III (days 31-39) due primarily to a negative effect of CO_2 on Nano-I abundances, as
422 depicted in the average 36 % reduction in Nano-I.

423 The temporal dynamics of Nano-II, the least abundant phytoplankton group analysed in our study,
424 displayed the largest variability (Fig. 3f), perhaps due to the spread of this cluster in flow cytographs
425 (which may indicate that this group represents several different phytoplankton species). No
426 significant relationship was found between net growth rate and $f\text{CO}_2$ for this group for the two
427 NMDS-based periods (Table 2, Figs S2f and S3f) nor with the peak in abundances on day 17 ($p=0.13$,
428 $R^2=0.46$; Fig. S4h). Moreover, no consistent trend was detected in mortality rates (Fig. 4f). Similar to
429 Nano-I, abundances in the surrounding water were often higher than in the mesocosms (max $3.5 \times$
430 10^2 ml^{-1} vs $1.1 \times 10^4 \text{ ml}^{-1}$, respectively; Figs. 3f and S6b).

431

432 **3.1.4 Algal carbon biomass**

433 The mean combined biomass of Pico-I and Pico-II showed a strong positive correlation with $f\text{CO}_2$
434 throughout the experiment ($p<0.05$, $R^2=0.95$; Fig. 5a), an effect already noticeable by day 2. Their
435 biomass in the high $f\text{CO}_2$ mesocosms was, on average 11 % higher than in the low $f\text{CO}_2$ mesocosms
436 between days 10-20 and 20 % higher between days 20-39. Conversely, the remaining algal groups
437 showed an average 10 % reduction in carbon biomass at enhanced $f\text{CO}_2$ (days 3-39, the sum of SYN,
438 Pico-III, Nano-I and II ; $p<0.01$; Fig. 5b). The most notable response was found for the biomass of
439 Pico-III, which showed an immediate negative response to CO_2 addition (Fig. S7a) and remained, on
440 average, 29 % lower throughout the study period (days 2-39). For Nano-I and II the lower carbon
441 biomass only became apparent during the end of Phase I and beginning of Phase II (days 14-20; Fig.

442 S7b). Due to its small cell size, the numerically dominant SYN accounted for an average of 40 % of
443 total carbon biomass.

444

445 **3.2 Prokaryote and virus population dynamics**

446 Prokaryote abundance in the mesocosms was positively related to total algal biomass independent of
447 treatment ($p < 0.05$, $R^2 = 0.33$; Fig. 8) and generally followed total algal biomass (Fig. S7c). The initial
448 increase in total prokaryote abundances occurred during the first few days following the closure of
449 the mesocosms (Fig. 6a). This was primarily due to increases in the HNA-prokaryote group (Fig. 6b)
450 which displayed higher net growth rates (0.22 d^{-1}) compared to the LNA-prokaryotes (0.14 d^{-1} on days
451 -3 to 3; Fig. 6c). A similar, albeit somewhat lower, increase was also recorded in the surrounding
452 waters (Fig. 6a). The decline of the first peak in prokaryote abundances coincided with the decay in
453 phytoplankton abundance/biomass (Figs. 1a and S7c). Concurrently the share of viral lysis increased,
454 representing 37-39 % of total mortality on day 11 (Fig. 7b). No measurable rates of lysogeny were
455 found for the prokaryotic community during the experimental period (all phases). From days 10 to 15
456 prokaryote dynamics (total, HNA and LNA) became noticeably affected by CO_2 concentration with a
457 significant positive correlation between net growth and $f\text{CO}_2$ during Phase I (days 3-13 NMDS-based
458 period 1; Table 2, Fig. S2 g and h). In the higher $f\text{CO}_2$ mesocosms, the decline in prokaryote
459 abundance occurring between days 13 and 16 (Fig. 6a) was largely (70 %) due to decreasing HNA-
460 prokaryote numbers (Fig. 6b). The grazing was 1.6-fold higher in the high $f\text{CO}_2$ mesocosm M3
461 compared to M1 (0.36 ± 0.13 and $0.14 \pm 0.08 \text{ d}^{-1}$ on day 14; Fig. 7a). At the same time, virus
462 abundance increased in the high $f\text{CO}_2$ mesocosms (Fig. 6d).

463 During Phase II, prokaryote abundances increased steadily until day 24 (for both HNA and LNA),
464 corresponding to increased algal biomass (Figs. 6 and S7c) and lowered grazing rates (Fig. 7a).
465 Specifically, during days 16-24 (NMDS-based period 2), the HNA-prokaryotes showed an average 10
466 % higher abundances in the low, as compared to the high $f\text{CO}_2$ mesocosms (Fig. 6b). However, a
467 significant negative correlation of net growth rates and $f\text{CO}_2$ was only found for LNA (Table 2, Fig S3g

468 and h). No significant differences in loss rates between M1 and M3 were found during Phase II
469 ($p=0.22$, 0.46 days 18 and 21 respectively; Fig. 7). Halfway through Phase II (day 24), the prokaryote
470 abundance in the surrounding water leveled off (Fig. 6a). Prokaryote abundance ultimately declined
471 during days 28-35 (Fig. 6a), whereby the net growth of LNA was again negatively correlated with
472 enhanced CO_2 ($p=0.02$, $R^2=0.76$; Table 2, Fig S3g). Unfortunately, no experimental data on grazing
473 and lysis of prokaryotes is present after day 25. However, viral abundances increased steadily at $2.2 \times$
474 10^6 d^{-1} , concomitant with a decline in prokaryote abundance (Fig. 6a and d). There was no significant
475 correlation between viral abundances and $f\text{CO}_2$ during Phases II and III ($p=0.36$, $R^2=0.21$).

476

477 **4 Discussion**

478 In most experimental mesocosm studies, nutrients have been added to stimulate phytoplankton
479 growth (Schulz et al., 2017) therefore little data exists for oligotrophic phytoplankton communities.
480 In this study, we describe the impact of increased $f\text{CO}_2$ on the brackish Baltic Sea microbial
481 community during summer (nutrient depleted; Paul et al., 2015). Small-sized phytoplankton
482 numerically dominated the autotrophic community, in particular SYN and Pico-I (both about $1 \mu\text{m}$
483 cell diameter). Our results demonstrate variable effects of $f\text{CO}_2$ manipulation on temporal
484 phytoplankton dynamics, dependent on phytoplankton group. In particular, Pico-I and Pico-II showed
485 significant positive responses, whilst the abundances of Pico-III, SYN and Nano-I were negatively
486 influenced by elevated $f\text{CO}_2$. The impact of OA on the different groups was, at times, a direct
487 consequence of alterations in gross growth rate, whilst overall phytoplankton population dynamics
488 could be explained by the combination of growth and losses. OA effects on community composition
489 in these systems may have consequences on both the food web and biogeochemical cycling.

490

491 **Comparison with surrounding waters**

492 During Phase 0, the microbial assemblage showed good replicability between all mesocosms,
493 however they had already begun to deviate from the community in the surrounding waters. This was

494 most likely a consequence of water movement altering the physical conditions and biological
495 composition of the surrounding water body. The dynamic nature of water movement in this region
496 has been shown to alter the entire phytoplankton community several times over within a few
497 months, due to fluctuations in nutrient supply, advection, replacement/mixing of water masses and
498 water temperature (Lips and Lips, 2010). Alternatively, effects of enclosure and the techniques
499 (bubbling) used to ensure a homogenous water column may have stimulated SYN within the
500 mesocosms, which has been found to occur in several mesocosm experiments (Paulino et al., 2008;
501 Gazeau et al., 2017). By Phases II and III, the microbial abundances within the mesocosms were
502 distinctly different from the surrounding waters, with generally fewer SYN and Pico-I, and more
503 Nano-I and Nano-II. Our statistical analysis shows that during this time, there was little similarity
504 between the surrounding waters and mesocosms regardless of the CO₂ treatment level. Thus, the
505 deviations during this time were most likely due to an upwelling event in the archipelago (days 17-
506 30; Paul et al., 2015). Cold, nutrient-rich deep water has been shown to upwell during summer, with
507 profound positive influence on ecosystem productivity (Nõmmann et al., 1991; Lehman and Myrberg,
508 2008). A relaxation from nutrient limitation in vertically stratified waters disproportionately favours
509 larger-sized phytoplankton, due to their higher nutrient requirements and lower capacity to compete
510 at low concentrations dictated by their lower surface to volume ratio (Raven, 1998; Veldhuis et al.,
511 2005). Inside the mesocosms, which were isolated from upwelled nutrients, picoeukaryotes
512 dominated similar to a stratified water column. Following this upwelling event, the pH of the
513 surrounding waters dropped from 8.3 to 7.8, a level comparable to the highest CO₂ treatment (M8)
514 on day 32 (Paul et al., 2015). Suggesting that other factors contributed to the observed differences
515 between mesocosms and surrounding water, than can be accounted for by CO₂ concentration alone
516 e.g. nutrients. Alternatively, the magnitude and source of mortality occurring in the surrounding
517 water may have been altered, compared to within the mesocosms, after such an upwelling event.
518 Although the grazer community in the surrounding waters was not studied during this campaign, it is
519 likely that the grazing community was completely restructured during the upwelling event (Uitto et

520 al., 1997). It is nonetheless noteworthy that the phytoplankton groups with distinct responses to CO₂
521 enrichment (either positive or negative) in the low (ambient) *f*CO₂ mesocosms diverged from those in
522 the surrounding water before the upwelling event occurred.

523

524 **Phytoplankton dynamics**

525 *Synechococcus* showed significantly lower net growth rates and peak abundances at higher *f*CO₂.
526 Both in laboratory and mesocosm experiments, *Synechococcus* has been reported to have diverse
527 responses to CO₂, with approximately equal accounts of positive (Lu et al., 2006; Schulz et al., 2017),
528 negative (Paulino et al., 2008; Hopkins et al., 2010; Traving et al., 2014,) and insignificant changes (Fu
529 et al., 2007; Lu et al., 2006) in net growth rate with *f*CO₂. This variable response is probably due, at
530 least in part, to the broad physiological and genetic diversity of this species. In the Gulf of Finland
531 alone, 46 different strains of *Synechococcus* were isolated in July 2004 (Haverkamp et al. 2009).
532 Direct effects on physiology have been implied from laboratory studies. One isolate, a phycoerythrin
533 rich strain of *Synechococcus* WH7803 (Traving et al., 2014) elicited a negative physiological effect on
534 the growth rate from increased CO₂. This was most likely a consequence of higher sensitivity to the
535 lower pH (Traving et al., 2014), and the cellular cost of maintaining pH homeostasis or conversely a
536 direct effect on protein export. Additionally, Lu et al. (2006) reported increased growth rates in a
537 cultured phycocyanin rich but not a phycoerythrin rich strain of *Synechococcus*, suggesting that
538 pigments may play some part in defining the direct physiological response within *Synechococcus*. In
539 addition, within natural communities (Paulino et al., 2008; Hopkins et al., 2010; Schulz et al., 2017)
540 variability can also arise from indirect effects such as altering competition with other picoplankton
541 (Paulino et al., 2008). The delay and dampened effect of *f*CO₂ on SYN abundances within our study
542 was more likely due to indirect effects arising from alterations in food web dynamics than to direct
543 impacts on the physiology of this species. Specifically, significant differences in grazing rates of SYN
544 between M1 and M3 (days 10 and 17, no significant lysis detected) could be responsible for the
545 differing dynamics between the mesocosms at the end of Phase I and beginning of Phase II.

546 The gross growth rates of Pico-I were significantly higher ($p < 0.05$) at high $f\text{CO}_2$ compared to the low
547 CO_2 concentrations during the first 10 days of Phase I. Moreover, no differences were detected in the
548 measured loss rates, demonstrating that increases in Pico-I were due to increases in growth
549 alone. The stimulation of Pico-I by elevated $f\text{CO}_2$ may be due to a stronger reliance on diffusive CO_2
550 entry compared to larger cells. Model simulations reveal that whilst near-cell CO_2/pH conditions are
551 close to those of the bulk water for cells $< 5 \mu\text{m}$ in diameter, they diverge as cell diameters increase
552 (Flynn et al., 2012). This is due to the size-dependent thickness of the diffusive boundary layer, which
553 determines the diffusional transport across the boundary layer and to the cell surface (Wolf-Gladrow
554 and Riebesell, 1997; Flynn et al., 2012). It is suggested that larger cells may be more able to cope
555 with $f\text{CO}_2$ variability as their carbon acquisition is more geared towards handling low CO_2
556 concentrations in their diffusive boundary layer, e.g. by means of active carbon acquisition and
557 bicarbonate utilization (Wolf-Gladrow and Riebesell, 1997; Flynn et al., 2012). Moreover, as the Baltic
558 Sea experiences particularly large seasonal fluctuations in pH and $f\text{CO}_2$ (Jansson et al., 2013) due to
559 the low buffering capacity of the waters, phytoplankton here are expected to have a higher degree of
560 physiological plasticity. Our results agree with previous mesocosm studies, which reported enhanced
561 abundances of picoeukaryotic phytoplankton (Brussaard et al., 2013; Davidson et al., 2016; Schulz et
562 al., 2017), and particularly the prasinophyte *Micromonas pusilla* at higher $f\text{CO}_2$ (Engel et al., 2007;
563 Meakin and Wyman, 2011). Furthermore, Schaum et al. (2012) found that 16 ecotypes of
564 *Ostreococcus tauri* (another prasinophyte similar in size to Pico-I) increased in growth rate by 1.4-1.7
565 fold at 1,000 compared to 400 $\mu\text{atm } f\text{CO}_2$. All ecotypes increased their photosynthetic rates and
566 those with most plasticity (those most able to vary their photosynthetic rate in response to changes
567 in $f\text{CO}_2$) were more likely to increase in frequency within the community. It is possible that Pico-I cells
568 are adapted to a highly variable carbonate system regime and are able to increase their
569 photosynthetic rate when additional CO_2 is available. This ability would allow them to out-compete
570 other phytoplankton (e.g. nanoeukaryotes in this study) in an environment when nutrients are
571 scarce.

572 The net growth rates and peak abundances of Pico-II were also positively affected by $f\text{CO}_2$. Gross
573 growth rates were significantly higher at high $f\text{CO}_2$ on only two occasions (days 10 and 20) and were
574 accompanied by high total mortality rates. Pigment analysis suggests that both Pico-I and Pico-II are
575 chlorophytes (Paul et al., 2015) and as such may share a common evolutionary history (Schulz et al.,
576 2017); thus Pico-II may be stimulated by $f\text{CO}_2$ in a similar manner to Pico I. Chlorophytes are found in
577 high numbers at this site throughout the year (Kuosa, 1991), suggesting the ecological relevance of
578 Pico-I and Pico-II in this ecosystem. In addition, Pico-II bloomed exactly when Pico-I declined which
579 may suggest potential competitive exclusion.

580 Pico-III showed the most distinct and immediate response to CO_2 addition. The significant reduction
581 in gross growth rates observed during Phase I suggests a direct negative effect of CO_2 on the
582 physiology of these cells. For this group, the lower gross growth rates were matched by lower total
583 mortality rates with increased $f\text{CO}_2$. Although the mean cell size of Pico-III and Pico-II were
584 comparable (2.9 and 2.5 μm , respectively), they showed opposing responses to $f\text{CO}_2$ enrichment
585 (lower Pico-III abundances at high $f\text{CO}_2$). These differences may arise from taxonomic differences
586 between the two groups. Pico-III displayed relatively high phycoerythrin orange autofluorescence,
587 likely representing small-sized cryptophytes (Klaveness, 1989), although rod-shaped *Synechococcus*
588 up to 2.9 μm in length (isolated from this region; Haverkamp et al., 2009) or *Synechococcus*
589 microcolonies (often only two cells in the Baltic; Motwani and Gorokhove, 2013) cannot be excluded.
590 In agreement with Pico-III response to CO_2 enrichment, Hopkins et al. (2010) reported reduced
591 abundances of small cryptophytes under increased CO_2 in a mesocosm study in a Norwegian fjord
592 near Bergen.

593 Lastly, the two nanoeukaryotic phytoplankton groups also displayed a negative response to $f\text{CO}_2$
594 enrichment, whereby Nano-II was the least defined, most likely due to a high taxonomic diversity in
595 this group. Nano-I started to display lower abundances at high $f\text{CO}_2$ during Phase I (after day 10),
596 which was likely the result of greater differences between gross growth and total mortality
597 (compared to low $f\text{CO}_2$). Alternatively, enhanced nutrient competition due to increased abundances

598 of SYN and Pico-I (and later on also Pico-II) at elevated $f\text{CO}_2$ may also have contributed to the
599 dampened response of Nano-I in the high $f\text{CO}_2$ mesocosms. The overall decline in Nano-I, during
600 Phase II, and sustained low abundances during Phase III may well have been the result of grazing by
601 the increased mesozooplankton abundances during Phase II (Lischka et al., 2017).

602

603 **Microbial loop**

604 The strong association of prokaryote abundance with algal biomass, present throughout the
605 experiment, suggests that the effect of CO_2 was an indirect consequence of alterations in the
606 availability of phytoplankton carbon. Others have reported a tight coupling of autotrophic and
607 heterotrophic communities at this location, with an estimated 35 % of the total net primary
608 production being utilized directly by bacteria or heterotrophic flagellates (Kuosa and Kivi, 1989),
609 suggesting a highly efficient microbial loop in this ecosystem. In addition to phytoplankton exudation,
610 viral lysis may also contribute to the dissolved organic carbon pool (Wilhelm and Suttle, 1999;
611 Brussaard et al., 2005; Lønborg et al., 2013). We calculated that viral lysis of phytoplankton between
612 days 9 and 13 resulted in the release of 1.3 and 13.1 ng C ml^{-1} for M1 and M3, respectively. Assuming
613 a bacterial growth efficiency of 30 % and cellular carbon conversion of 7 fg C cell^{-1} (Hornick et al.,
614 2017), we estimate that the organic carbon required to support bacterial dynamics during this period
615 (taking into account the net growth and loss rates) was 2.9 and 11.5 ng C ml^{-1} in low and high $f\text{CO}_2$
616 mesocosms M1 and M3, respectively. These results suggest that viral lysis of phytoplankton was an
617 important source of organic carbon for the bacterial community. Our results are consistent with
618 bacterial-phytoplankton coupling during this eastern Baltic Sea mesocosm study (Hornick et al.,
619 2017), and agree with earlier work on summer carbon flow in the northern Baltic Sea showing that
620 prokaryotic growth was largely supported by recycled carbon (Uitto et al., 1997). The average net
621 growth rates of the prokaryotes during the first period of increase in Phases 0 and I (0.2 d^{-1}) were
622 comparable to rates reported for this region (Kuosa, 1991). In order to sustain the concomitant daily
623 mortality (between $0.3\text{-}0.5 \text{ d}^{-1}$) measured during our study, prokaryotic gross growth rates must have

624 been close to one doubling a day ($0.5-0.7 \text{ d}^{-1}$). During Phase I, grazing was the dominant loss factor of
625 the prokaryotic community although there was also evidence that viral lysis was occurring.
626 Bermúdez et al. (2016) reported the highest biomass of protozoans around day 15. This was
627 predominantly the heterotrophic choanoflagellate *Calliakantha natans*, which selectively feeds on
628 particles $<1 \mu\text{m}$ in diameter (Marchant and Scott, 1993; Hornick et al., 2017). Indeed, an earlier study
629 in this area showed that heterotrophic nanoflagellates were the dominant grazers of bacteria,
630 responsible for ingestion of approximately 53 % of bacterial production compared to only 11 % being
631 grazing by ciliates (Uitto et al., 1997). During the first half of Phase II, grazing was reduced and likely
632 contributed to the steady increase in prokaryote abundances. Specifically, a negative relationship
633 between the abundances of HNA-prokaryotes and $f\text{CO}_2$ was detected and corresponded to reduced
634 bacterial production and respiration at higher $f\text{CO}_2$ (Hornick et al., 2017; Spilling et al., 2016).
635 Although CO_2 enrichment may not directly affect bacterial growth, co-occurring global rise in
636 temperature can increase enzyme activities, affecting bacterial production and respiration rates
637 (Piontek et al., 2009; Wohlers et al., 2009; Wohlers-Zöllner et al., 2011). Enhanced bacterial re-
638 mineralization of organic matter may stimulate autotrophic production by the small-sized
639 phytoplankton (Riebesell et al., 2009; Riebesell and Tortell, 2011; Engel et al., 2013), intensifying the
640 selection of small cell size.

641 Mean viral abundances were higher under CO_2 enrichment towards the end of Phase I and into Phase
642 II which is expected under conditions of increased phytoplankton and prokaryote biomass. The
643 estimated average viral burst size, obtained from this increase in total viral abundance and
644 concurrent decline in bacterial abundances, was about 30 which is comparable to published values
645 (Parada et al, 2006; Wommack and Colwell, 2000). Viral lysis rates of prokaryotes were measured
646 until day 25 and indicated that during days 18-25 an average 10-15 % of the total prokaryote
647 population was lysed per day. Moreover, the concurrent steady increase in viral abundances during
648 Phase III indicates that viral lysis of the prokaryotes remained important. Thus, the combined impact
649 of increased viral mortality together with reduced production (Hornick et al., 2017) ultimately led to

650 the decline in prokaryote abundance (this study). Lysogeny did not appear to be an important life
651 strategy of viruses during our campaign. Direct effects of higher $f\text{CO}_2$ on viruses are not expected, as
652 marine virus isolates are quite stable (both in terms of particle decay and loss of infectivity) over the
653 range of pH of the present study (Danovaro et al., 2011; Mojica and Brussaard, 2014). The few
654 studies which have inferred viral lysis rates based on changes in viral abundances show reduced
655 abundances of algal viruses (e.g. *Emiliania huxleyi* virus) under enhanced CO_2 (Larsen et al., 2008)
656 while mesocosm results by Brussaard et al. (2013) indicated a stronger impact of viruses on bacterial
657 abundance dynamics with CO_2 enrichment.

658

659 **5 Conclusions**

660 Due to the low buffering capacity of the Baltic Sea and the paucity of data regarding OA impact in
661 nutrient-limited waters, the results presented here are pertinent to increasing our understanding of
662 how projected rises in $f\text{CO}_2$ will affect the microbial communities in this region. Our study provides
663 evidence that cell size, taxonomy and sensitivity to loss can all play a role in the outcome of CO_2
664 enrichment. Physiological constraints of cell size favour nutrient uptake by small cells under
665 conditions of reduced nutrients and our results show that these effects can be further exacerbated
666 by OA. Gross growth rates along with the complementary mortality rates allowed for a more
667 comprehensive understanding of the phytoplankton population dynamics and thus perception of
668 how microbial food web dynamics can influence the response of the autotrophic and heterotrophic
669 components of the community. Our results further suggest that alterations in CO_2 concentrations are
670 expected to affect prokaryote communities (mainly) indirectly through alterations in phytoplankton
671 biomass, productivity and viral lysis. Overall, the combination of growth and losses (grazing and viral
672 lysis) could explain microbial population dynamics observed in this study. It is noteworthy to
673 mention, a recent study in the oligotrophic northeast Atlantic Ocean reported a shift from grazing-
674 dominated to viral lysis-dominated phytoplankton community with strengthening of vertical
675 stratification (shoaling the mixed layer depth and enhancing nutrient limitation) (Mojica et al., 2016).

676 Thus, we highly recommend that future research on OA combine mesocosm studies focusing on
677 changes in microbial community composition and activity with experiments aimed at understanding
678 the effects of OA on food web dynamics, i.e. partitioning mortality between grazing and viral lysis
679 (Brussaard et al., 2008).

680

681 **Author Contribution**

682 Design and overall coordination of research by CB. Organization and performance of analyses in the
683 field by KC. Data analysis by KC, CB, and SA-F. Design and coordination of the overall KOSMOS
684 mesocosm project by UR. All authors contributed to the writing of the paper (KC, KM and CB are lead
685 authors).

686

687 **Acknowledgements**

688 This project was funded through grants to C.B. by the Darwin project, the Netherlands Institute for
689 Sea Research (NIOZ), and the EU project MESOAQUA (grant agreement number 228224). We thank
690 the KOSMOS project organisers and team, in particular Andrea Ludwig, the staff of the Tvärminne
691 Zoological Station and the diving team. We give special thanks to Anna Noordeloos, Kirsten Kooijman
692 and Richard Doggen for their technical assistance during this campaign. We also gratefully
693 acknowledge the captain and crew of R/V ALKOR for their work transporting, deploying and
694 recovering the mesocosms. The collaborative mesocosm campaign was funded by BMBF projects
695 BIOACID II (FKZ 03F06550) and SOPRAN Phase II (FKZ 03F0611).

696

697

References

- Aberle, N., Schulz, K., Stuhr, A., Malzahn, A., Ludwig, A. and Riebesell, U.: High tolerance of microzooplankton to ocean acidification in an Arctic coastal plankton community, *Biogeosciences*, 10, 1471–1481, doi:10.5194/bg-10-1471-2013, 2013.
- Barcelos e Ramos, J., Biswas, H., Schulz, K. G., LaRoche, J. and Riebesell, U.: Effect of rising atmospheric carbon dioxide on the marine nitrogen fixer *Trichodesmium*, *Global Biogeochem. Cycles*, 21(2), doi:10.1029/2006GB002898, 2007.
- Baudoux, A. C., Noordeloos, A. A. M., Veldhuis, M. J. W. and Brussaard, C. P. D.: Virally induced mortality of *Phaeocystis globosa* during two spring blooms in temperate coastal waters, *Aquat. Microb. Ecol.*, 44(3), 207–217, doi:10.3354/ame044207, 2006.
- Bermúdez, J., Winder, M., Stuhr, A., Almén, A., Engström-Öst, J. and Riebesell, U.: Effect of ocean acidification on the structure and fatty acid composition of a natural plankton community in the Baltic Sea, *Biogeosciences*, 13, 6625–6635, doi:10.5194/bg-13-6625-2016, 2016
- Brussaard, C. P. D.: Optimization of Procedures for Counting Viruses by Flow Cytometry, *Appl. Environ. Microbiol.*, 70(3), 1506–1513, doi:10.1128/AEM.70.3.1506-1513.2004, 2004.
- Brussaard, C. P. D., Kuipers, B. and Veldhuis, M. J. W.: A mesocosm study of *Phaeocystis globosa* population dynamics: I. Regulatory role of viruses in bloom control, *Harmful Algae*, 4(5), 859–874, doi:10.1016/j.hal.2004.12.015, 2005.
- Brussaard, C. P. D., Wilhelm, S. W., Thingstad, F., Weinbauer, M. G., Bratbak, G., Heldal, M., Kimmance, S. A., Middelboe, M., Nagasaki, K., Paul, J. H., Schroeder, D. C., Suttle, C. A., Vaqué, D. and Wommack, K. E.: Global-scale processes with a nanoscale drive: the role of marine viruses., *ISME J.*, 2(6), 575–578, doi:10.1038/ismej.2008.31, 2008.
- Brussaard, C. P. D., Noordeloos, A. A. M., Witte, H., Collenteur, M. C. J., Schulz, K., Ludwig, A. and Riebesell, U.: Arctic microbial community dynamics influenced by elevated CO₂ levels, *Biogeosciences*, 10, 719–731, doi:10.5194/bg-10-719-2013, 2013.
- Clarke, K.R.: Non-parametric multivariate analyses of changes in community structure. *Aust. J. Ecol.*, 18, 117-143, 1993.
- Corno, G., Karl, D., Church, M., Letelier, R., Lukas, R., Bidigare, R. and Abbott, M.: Impact of climate forcing on ecosystem processes in the North Pacific Subtropical Gyre, *J. Geophys. Res.*, 112, 1-14, 2007.
- Danovaro, R., Corinaldesi, C., Dell'Anno, A., Fuhrman, J. A., Middelburg, J. J., Noble, R. T. and Suttle, C. A.: Marine viruses and global climate change, *FEMS Microbiol. Rev.*, 35, 993–1034, 2011.
- Davidson, A., McKinlay, J., Westwood, K., Thomson, P., Van Den Enden, R., De Salas, M., Wright, S., Johnson, R. and Berry, K.: Enhanced CO₂ concentrations change the structure of Antarctic marine microbial communities, *Mar. Ecol. Progr. Ser.*, 552, 93–113. doi: 10.3354/meps11742, 2016.

- Doney, S. C., Fabry, V. J., Feely, R. A. and Kleypas, J. A.: Ocean acidification: The other CO₂ problem, *Annu. Rev. Mar. Sci.*, 1, 169–192, 2009.
- Dutkiewicz, S., Morris, J.J., Follows, M.J., Scott, J., Levitan, O., Dyhrman, S.T., and Berman-Frank, I.: Impact of ocean acidification on the structure of future phytoplankton communities, *Nat. Clim. Change*, 5(11), 1002-1006, 2015.
- Eberlein, T., Wohlrab, S., Rost, B., John, U., Bach, L. T., Riebesell, U. and Van de Waal, D. B.: Effects of ocean acidification on primary production in a coastal North Sea phytoplankton community, *PLoS ONE*, 12 (3). e0172594. DOI 10.1371/journal.pone.0172594, 2017.
- Engel, A., Schulz, K., Riebesell, U., Bellerby, R., Delille, B. and Schartau, M.: Effects of CO₂ on particle size distribution and phytoplankton abundance during a mesocosm bloom experiment (PeECE II), *Biogeosciences*, 5, 509–521, doi:10.5194/bgd-4-4101-2007, 2007.
- Engel, A., Borchard, C., Piontek, J., Schulz, K. G., Riebesell, U. and Bellerby, R.: CO₂ increases ¹⁴C primary production in an Arctic plankton community, *Biogeosciences*, 10(3), 1291–1308, doi:10.5194/bg-10-1291-2013, 2013.
- Evans, C. and Brussaard, C.P.D.: Regional variation in lytic and lysogenic viral infection in the Southern Ocean and its contribution to biogeochemical cycling. *Appl. Environ. Microbiol.*, 78 (18), 6741-6748, 2012.
- Feng, Y., Leblanc, K., Rose, J. M., Hare, C. E., Zhang, Y., Lee, P. A., Wilhelm, S. W., DiTullio, G. R., Rowe, J. M., Sun, J., Nemcek, N., Gueguen, C., Passow, U., Benner, I., Hutchins, D. A. and Brown, C.: Effects of increased pCO₂ and temperature on the North Atlantic spring bloom. I. The phytoplankton community and biogeochemical response, *Mar. Ecol. Progr. Ser.*, 388, 13–25, doi: 10.3354/meps08133, 2009.
- Field, C. B., Behrenfeld, M. J., Randerson, J. T. and Falkowski, P.: Primary Production of the Biosphere: Integrating Terrestrial and Oceanic Components, *Science*, 281(5374), 237–240, doi:10.1126/science.281.5374.237, 1998.
- Flynn, K. J., Blackford, J. C., Baird, M. E., Raven, J. A., Clark, D. R., Beardall, J., Brownlee, C., Fabian, H. and Wheeler, G. L.: Letter. Changes in pH at the exterior surface of plankton with ocean acidification, *Nat. Clim. Change*, 2(7), 510–513, doi:10.1038/nclimate1696, 2012.
- Fu, F. X., Warner, M. E., Zhang, Y., Feng, Y. and Hutchins, D. A.: Effects of increased temperature and CO₂ on photosynthesis, growth, and elemental ratios in marine *Synechococcus* and *Prochlorococcus* (Cyanobacteria), *J. Phycol.*, 43(3), 485–496, doi:10.1111/j.1529-8817.2007.00355.x, 2007.
- Garrison, D. L., Gowing, M. M., Hughes, M. P., Campbell, L., Caron, D. A., Dennett, M. R., Shalapyonok, A., Olson, J. A., Landry, M. R., Brown, S. L., Liu, H-B., Azam, F., Steward, G. F., Ducklow, H. W. and Smith, D. C.: Microbial food web structure in the Arabian Sea: A US JGOFS study. *Deep-Sea Res. Part II*, 47, 1387-1422, doi:10.1016/S0967-0645(99)00148-4, 2000.
- Gazeau, F., Sallon, A., Pitta, P., Tsiola, A., Maugeudre, L., Giani, M., Celussi, M., Pedrotti, M. L., Marro, S. and Guieu, C.: Limited impact of ocean acidification on phytoplankton community structure and carbon export in an oligotrophic environment: results from two short-term mesocosm

studies in the Mediterranean Sea. *Estuar. Coast. Shelf Sci.* 186, 72–88, doi:10.1016/j.ecss.2016.11.016, 2017.

Gruber, N.: Warming up, turning sour, losing breath: Ocean biogeochemistry under global change, *Phil. Trans. R. Soc. A*, 369, 1980–1996, 2011.

Haverkamp, T., Schouten, D., Doeleman, M., Wollenzien, U., Huisman, J. and Stal, L.: Colorful microdiversity of *Synechococcus* strains (picocyanobacteria) isolated from the Baltic Sea, *ISME J.*, 3, 397–408, 2009.

Hein, M. and Sand-Jensen, K.: CO₂ increases oceanic primary production, *Nature*, 388(6642), 526–527, 1997.

Hopkins, F. E., Turner, S. M., Nightingale, P. D., Steinke, M., Bakker, D., and Liss, P. S.: Ocean acidification and marine trace gas emissions, *P. Natl. Acad. Sci. USA*, 107, 760–765, doi:10.1073/pnas.0907163107, 2010.

Hornick, T., Bach, L. T., Crawford, K. J., Spilling, K., Achterberg, E. P., Brussaard, C. P. D., Riebesell, U., and Grossart, H.-P.: Ocean acidification indirectly alters trophic interaction of heterotrophic bacteria at low nutrient conditions, *Biogeosciences*, 14, 1–15, doi:10.5194/bg-2016-61, 2017.

Hutchins, D. A., Fe, F.-X., Zhang, Y., Warner, M. E., Feng, Y., Portune, K., Bernhardt, P. W. and Mulholland, M. R.: CO₂ control of *Trichodesmium* N₂ fixation, photosynthesis, growth rates, and elemental ratios: implications for past, present, and future ocean biogeochemistry, *Limnol. Oceanogr.*, 52(4), 1293–1304, 2007.

Jansson, A., Norkko, J. and Norkko, A.: Effects of Reduced pH on *Macoma balthica* Larvae from a System with Naturally Fluctuating pH-Dynamics, *PLoS One*, 8(6), doi:10.1371/journal.pone.0068198, 2013.

Kimance, S. A. and Brussaard, C. P. D.: Estimation of viral-induced phytoplankton mortality using the modified dilution method, in: *Manual of Aquatic Viral Ecology*, edited by: Wilhelm S. W., Weinbauer M., Suttle C. A., pp 65–73, ASLO, 2010.

Klaveness, D.: Biology and ecology of the Cryptophyceae: status and challenges., *Biol Ocean.*, 6, 257–270, 1989.

Kulinski, K. and Pempkowiak, J.: The carbon budget of the Baltic Sea, *Biogeosciences*, 8, 4841–4869, 2011.

Kuosa, H.: Picoplanktonic algae in the northern Baltic Sea: seasonal dynamics and flagellate grazing, *Mar. Ecol. Prog. Ser.*, 73(2-3), 269–276, doi:10.3354/meps073269, 1991.

Kuosa, H. and Kivi, K.: Bacteria and heterotrophic flagellates in the pelagic carbon cycle in the northern Baltic Sea, *Mar. Ecol. Prog. Ser.*, 53, 93–100, doi:10.3354/meps053093, 1989.

Larsen, J. B., Larsen, A., Thyraug, R., Bratbak, G. and Sandaa, R. A.: Response of marine viral populations to a nutrient induced phytoplankton bloom at different pCO₂ levels, *Biogeosciences*, 5, 523–533, doi:10.5194/bg-5-523-2008, 2008.

- Legendre, P., and Legendre, L.: Numerical Ecology. Amsterdam; New York: Elsevier, 1998.
- Lehmann, A. and Myrberg, K.: Upwelling in the Baltic Sea – A review, *J. Marine Syst.*, 74, S3–S12, doi:10.1016/j.jmarsys.2008.02.010, 2008.
- Leonardos, N. and Geider, R. J.: Elevated atmospheric carbon dioxide increases organic carbon fixation by *Emiliana huxleyi* (Haptophyta), under nutrient-limited high-light conditions, *J. Phycol.*, 41(6), 1196–1203, doi:0.1111/j.1529-8817.2005.00152.x, 2005.
- Lips, I. and Lips, U.: Phytoplankton dynamics affected by the coastal upwelling events in the Gulf of Finland in July–August 2006. *J. Plankton Res.*, 32 (9), 1269–1282, 2016.
- Lischka, S., Bach, L.T., Schulz, K.G. and Riebesell, U.: Micro- and mesozooplankton community response to increasing levels of fCO₂ in the Baltic Sea: insights from a large-scale mesocosm experiment, *Biogeosciences*, 14, 447–466, doi:10.5194/bg-14-447-2017, 2017.
- Lønborg, C., Middelboe, M. and Brussaard, C. P. D.: Viral lysis of *Micromonas pusilla*: Impacts on dissolved organic matter production and composition, *Biogeochemistry*, 116(1-3), 231–240, doi:10.1007/s10533-013-9853-1, 2013.
- Lu, Z., Jiao, N. and Zhang, H.: Physiological changes in marine picocyanobacterial *Synechococcus* strains exposed to elevated CO₂ partial pressure, *Mar. Biol. Res.*, 2(6), 424–430, doi:10.1080/17451000601055419, 2006.
- Marchant, H.J. and Scott F.J.: Uptake of sub-micrometre particles and dissolved organic material by Antarctic choanoflagellates, *Mar. Ecol. Prog. Ser.*, 92, 59–64, 1993.
- Marie, D., Brussaard, C. P. D., Thyrhaug, R., Bratbak, G. and Vaultot, D.: Enumeration of marine viruses in culture and natural samples by flow cytometry, *Appl. Environ. Microbiol.*, 65(1), 45–52, 1999.
- Meakin, N. G. and Wyman, M.: Rapid shifts in picoeukaryote community structure in response to ocean acidification., *ISME J.*, 5(9), 1397–405, doi:10.1038/ismej.2011.18, 2011.
- Meyer, J. and Riebesell, U.: Reviews and Syntheses: Responses of coccolithophores to ocean acidification: a meta-analysis, *Biogeosciences*, 12(6), 1671–1682, doi:10.5194/bg-12-1671-2015, 2015.
- Middelboe, M. and Lyck, P. G.: Regeneration of dissolved organic matter by viral lysis in marine microbial communities, *Aquat. Microb. Ecol.*, 27(2), 187–194, doi:10.3354/ame027187, 2002.
- Mojica, K. D. A., Evans, C. and Brussaard, C. P. D.: Flow cytometric enumeration of marine viral populations at low abundances, *Aquat. Microb. Ecol.*, 71(3), 203–209, doi:10.3354/ame01672, 2014.
- Mojica, K. D. A. and Brussaard, C. P. D.: Factors affecting virus dynamics and microbial host–virus interactions in marine environments, *FEMS Microbiol. Ecol.*, 89(3), 495–515, doi:10.1111/1574-6941.12343, 2014.

Mojica, K. D. A., Huisman, J., Wilhelm, S. W. and Brussaard, C. P. D.: Latitudinal variation in virus-induced mortality of phytoplankton across the North Atlantic Ocean, *ISME J.*, doi:10.1038/ismej.2015.130, 2016.

Motwani, N., and Gorokhova, E.: Mesozooplankton grazing on picocyanobacteria in the Baltic Sea as inferred from molecular diet analysis, *PLoS ONE*, 8: e79230, 2013.

Niehoff, B., Schmithüsen, T., Knüppel, N., Daase, M., Czerny, J., and Boxhammer, T.: Mesozooplankton community development at elevated CO₂ concentrations: results from a mesocosm experiment in an Arctic fjord, *Biogeosciences*, 10, 1391–1406, doi:10.5194/bg-10-1391-2013, 2013.

Nömmann, S., Sildam, J., Nöges, T. and Kahru, M.: Plankton distribution during a coastal upwelling event off Hiiumaa, Baltic Sea: impact of short-term flow field variability. *Cont. Shelf Res.*, 11 (1), 95-108, 1991.

Oksanen, J., Blanchet, F. G., Friendly, M., Kindt, R., Legendre, P., McGlenn, D., Minchin, P., R., O'Hara, R. B., L. Simpson, G. L., Solymos, P., Stevens, M. H. H., Szoecs, E. and Wagner, H.: *vegan: Community Ecology Package*. R package version 2.4-3. <https://CRAN.R-project.org/package=vegan>, 2017.

Parada, V., Herndl, G. and Weinbauer, M.: Viral burst size of heterotrophic prokaryotes in aquatic systems. *J. Mar. Biol. Assoc. U. K.*, 86, 613-621, doi:10.1017/S002531540601352X, 2006.

Paul, A. J., Bach, L. T., Boxhammer, T., Czerny, J., Hellemann, D., Trense, Y., Nausch, M., Sswat, M., Riebesell, U., Road, M., Lismore, E. and Way, E.: Effect of elevated CO₂ on organic matter pools and fluxes in a summer, post spring-bloom Baltic Sea plankton community, *Biogeosciences*, 12, 6181–6203, doi: 10.5194/bg-12-6181-2015, 2015.

Paulino, A. I., Egge, J. K. and Larsen, A.: Effects of increased atmospheric CO₂ on small and intermediate sized osmotrophs during a nutrient induced phytoplankton bloom, *Biogeosciences Discuss.*, 4(6), 4173–4195, doi:10.5194/bgd-4-4173-2007, 2008.

Pfeil, B., Olsen, A., Bakker, D. C. E., Hankin, S., Koyuk, H., Kozyr, A., Malczyk, J., Manke, A., Metzl, N., Sabine, C. L., Akl, J., Alin, S. R., Bates, N., Bellerby, R. G. J., Borges, A., Boutin, J., Brown, P. J., Cai, W. J., Chavez, F. P., Chen, A., Cosca, C., Fassbender, A. J., Feely, R. A., González-Dávila, M., Goyet, C., Hales, B., Hardman-Mountford, N., Heinze, C., Hood, M., Hoppema, M., Hunt, C. W., Hydes, D., Ishii, M., Johannessen, T., Jones, S. D., Key, R. M., Körtzinger, A., Landschützer, P., Lauvset, S. K., Lefèvre, N., Lenton, A., Lourantou, A., Merlivat, L., Midorikawa, T., Mintrop, L., Miyazaki, C., Murata, A., Nakadate, A., Nakano, Y., Nakaoka, S., Nojiri, Y., Omar, A. M., Padin, X. A., Park, G. H., Paterson, K., Perez, F. F., Pierrot, D., Poisson, A., Ríos, A. F., Santana-Casiano, J. M., Salisbury, J., Sarma, V. V. S. S., Schlitzer, R., Schneider, B., Schuster, U., Sieger, R., Skjelvan, I., Steinhoff, T., Suzuki, T., Takahashi, T., Tedesco, K., Telszewski, M., Thomas, H., Tilbrook, B., Tjiputra, J., Vandemark, D., Veness, T., Wanninkhof, R., Watson, A., Weiss, R., Wong, C. and Yoshikawa-Inoue, H.: A uniform, quality controlled Surface Ocean CO₂ Atlas (SOCAT), *Earth Syst. Sci. Data Discuss.*, 5 (2), 735-780, doi: 10.5194/essdd-5-735-2012, 2012.

Pinheiro, J., Bates, D., DebRoy, S., Sarkar, D. and R Core Team.: *nlme: Linear and Nonlinear Mixed Effects Models*. R package version 3.1-131, <https://CRAN.R-project.org/package=nlme>, 2017.

- Piontek, J., Händel, N., Langer, G., Wohlers, J., Riebesell, U. and Engel, A.: Effects of rising temperature on the formation and microbial degradation of marine diatom aggregates, *Aquat. Microb. Ecol.*, 54, 305–318, doi:10.3354/ame01273, 2009.
- Qiu, B. and Gao, K.: Effects of CO₂ enrichment on the bloom-forming cyanobacterium *Microcystis aeruginosa* (Cyanophyceae): Physiological responses and relationships with the availability of dissolved inorganic carbon, *J. Phycol.*, 38(4), 721–729, doi:10.1046/j.1529-8817.2002.01180.x, 2002.
- R Core Team, R: A language and environment for statistical computing. R Foundation for Statistical Computing, Vienna, Austria. URL <https://www.R-project.org/>, 2017.
- Raven, J. A.: The twelfth Tansley Lecture. Small is beautiful: The picophytoplankton, *Funct. Ecol.*, doi:10.1046/j.1365-2435.1998.00233.x, 1998.
- Riebesell, U., Körtzinger, A. and Oschlies, A.: Sensitivities of marine carbon fluxes to ocean change, *Proc. Natl. Acad. Sci. U. S. A.*, 106(49), 20602–20609, doi:10.1073/pnas.0813291106, 2009.
- Riebesell, U. and Tortell, P. D.: Effects of ocean acidification on pelagic organisms and ecosystems, in: *Ocean Acidification*, edited by: Gattuso, J.-P. and Hansson, L., p. 99, Oxford University Press, Oxford, United Kingdom, 2011.
- Riebesell, U., Czerny, J., von Bröckel, K., Boxhammer, T., Büdenbender, J., Deckelnick, M., Fischer, M., Hoffmann, D., Krug, S.A., Lentz, U., Ludwig, A., Mücke, R. and Schulz, K. G.: Technical Note: A mobile sea-going mesocosm system – new opportunities for ocean change research, *Biogeosciences*, 10, 1835–1847, doi:10.5194/bg-10-1835-2013, 2013.
- Riebesell, U., Bach, L. T., Bellerby, R. G. J., Bermudez, R., Boxhammer, T., Czerny, J., Larsen, A., Ludwig, A. and Schulz, K. G.: Ocean acidification impairs competitive fitness of a predominant pelagic calcifier, *Nature Geoscience*, 10, 19–24, doi:10.1038/ngeo2854, 2017.
- Rose, J. M., Feng, Y., Gobler, C. J., Gutierrez, R., Harel, C. E., Leblancl, K. and Hutchins, D. A.: Effects of increased pCO₂ and temperature on the North Atlantic spring bloom. II. Microzooplankton abundance and grazing, *Mar. Ecol. Prog. Ser.*, 388, 27–40, doi:10.3354/meps08134, 2009.
- Schaum, E., Rost, B., Millar, A. J. and Collins, S.: Variation in plastic responses of a globally distributed picoplankton species to ocean acidification, *Nat. Clim. Change*, 3, 298–302. doi: 10.1038/nclimate1774, 2012.
- Schulz, K. G. and Riebesell, U.: Diurnal changes in seawater carbonate chemistry speciation at increasing atmospheric carbon dioxide, *Mar. Biol.*, 160, 1889–1899, doi:10.1007/s00227-012-1965-y, 2013.
- Schulz, K., Bach, L., Bellerby, R., Bermúdez, R., Büdenbender, J., Boxhammer, T., Czerny, J., Engel, A., Ludwig, A., Meyerhöfer, M., Larsen, A., Paul, A., Sswat, M.I., Riebesell, U.: Phytoplankton Blooms at Increasing Levels of Atmospheric Carbon Dioxide: Experimental Evidence for Negative Effects on Prymnesiophytes and Positive on Small Picoeukaryotes, *Frontiers in Marine Science*, 4, 64, 2017.

Sheik, A. R., Brussaard, C. P. D., Lavik, G., Lam, P., Musat, N., Krupke, A., Littmann, S., Strous, M. and Kuypers, M. M. M.: Responses of the coastal bacterial community to viral infection of the algae *Phaeocystis globosa*, *ISME J.*, 8(1), 212–25, doi:10.1038/ismej.2013.135, 2014.

Sherr, E.B., Caron, D. A. and B. F. Sherr.: Staining of heterotrophic protists for visualization via epifluorescence microscopy, in: *Current Methods in Aquatic Microbial Ecology*, edited by: B. Sherr, E. Sherr and J. C. P. Kemp, pp. 213–228, Lewis Publ., N.Y., 1993.

Spilling, K., Paul, A. J., Virkkala, N., Hastings, T., Lischka, S., Stuhr, A., Bermudez, R., Czerny, J., Schulz, K. G., Ludwig, A. and Riebesell, U.: Ocean acidification decreases plankton respiration: evidence from a mesocosm experiment, *Biogeosciences*, 13, 4707–4719, 2016.

Stoecker, D. K., Nejstgaard, J., Madhusoodhanan, R. and Larsen, A.: Underestimation of microzooplankton grazing in dilution experiments due to inhibition of phytoplankton growth, *Limnol. Oceanogr.*, 60, 1426–1438, doi:10.1002/lno.10106, 2015.

Suffrian, K., Simonelli, P., Nejstgaard, J. C., Putzeys, S., Carotenuto, Y. and Antia, A. N.: Microzooplankton grazing and phytoplankton growth in marine mesocosms with increased CO₂ levels, *Biogeosciences*, 5, 1145–1156, 2008.

Tortell, P. D., DiTullio, G. R., Sigman, D. M. and Morel, F. M. M.: CO₂ effects on taxonomic composition and nutrient utilization in an Equatorial Pacific phytoplankton assemblage, *Mar. Ecol. Prog. Ser.*, 236, 37–43, 2002.

Traving, S. J., Clokie, M. R. J. and Middelboe, M.: Increased acidification has a profound effect on the interactions between the cyanobacterium *Synechococcus* sp. WH7803 and its viruses, *FEMS Microbiol. Ecol.*, 87(1), 133–141, doi:10.1111/1574-6941.12199, 2014.

Turley, C. and Boot, K.: UNEP emerging issues: Environmental consequences of ocean acidification: A threat to food security, *United Nations Environ. Program.*, 2010.

Uitto, A., Heiskanen, A., Lignell, R., Autio, R., and Pajuniemi, R.: Summer dynamics of the coastal planktonic food web in the northern Baltic Sea, *Mar. Ecol. Prog. Ser.*, 151, 27–41, doi:10.3354/meps151027, 1997.

Veldhuis, M. J. W. and Kraay, G. W.: Phytoplankton in the subtropical Atlantic Ocean: Towards a better assessment of biomass and composition, *Deep. Res. Part I Oceanogr. Res. Pap.*, 51(4), 507–530, doi:10.1016/j.dsr.2003.12.002, 2004.

Veldhuis, M. J. W., Timmermans, K. R., Croot, P. and Van Der Wagt, B.: Picophytoplankton; A comparative study of their biochemical composition and photosynthetic properties, *J. Sea Res.*, 53(1-2 SPEC. ISS.), 7–24, doi:10.1016/j.seares.2004.01.006, 2005.

Weinbauer, M. G.: Ecology of prokaryotic viruses, *FEMS Microbiol. Rev.*, 28(2), 127–181, doi:10.1016/j.femsre.2003.08.001, 2004.

Weinbauer, M. G. and Suttle, C. A.: Potential significance of lysogeny to bacteriophage production and bacterial mortality in coastal waters of the Gulf of Mexico, *Appl. Environ. Microbiol.*, 62(12), 4374–4380, 1996.

Weinbauer, M. G., Mari, X. and Gattuso, J.-P.: Effect of ocean acidification on the diversity and activity of heterotrophic marine microorganisms, in: *Ocean Acidification*, edited by: Gattuso, J.-P. and Hansson, L., p. 83-98, Oxford University Press, Oxford, United Kingdom, 2011.

Wilhelm, S. W. and Suttle, C. A.: Viruses and Nutrient Cycles in the Sea aquatic food webs, *Bioscience*, 49(10), 781–788, doi:10.2307/1313569, 1999.

Wilhelm, S. W., Brigden, S. M. and Suttle, C. A.: A dilution technique for the direct measurement of viral production: A comparison in stratified and tidally mixed coastal waters, *Microb. Ecol.*, 43(1), 168–173, doi:10.1007/s00248-001-1021-9, 2002.

Winget, D. M., Williamson, K. E., Helton, R. R. and Wommack, K. E.: Tangential flow diafiltration: An improved technique for estimation of virioplankton production, *Aquat. Microb. Ecol.*, 41(3), 221–232, doi:10.3354/ame041221, 2005.

Wohlers, J., Engel, A., Zöllner, E., Breithaupt, P., Jürgens, K., Hoppe, H.-G., Sommer, U. and Riebesell, U.: Changes in biogenic carbon flow in response to sea surface warming., *Proc. Natl. Acad. Sci. U. S. A.*, 106(17), 7067–7072, doi:10.1073/pnas.0812743106, 2009.

Wohlers-Zöllner, J., Breithaupt, P., Walther, K., Jürgens, K. and Riebesell, U.: Temperature and nutrient stoichiometry interactively modulate organic matter cycling in a pelagic algal-bacterial community, *Limnol. Oceanogr.*, 56(2), 599–610, doi:10.4319/lo.2011.56.2.0599, 2011.

Wolf-Gladrow, D. and Riebesell, U.: Diffusion and reactions in the vicinity of plankton: A refined model for inorganic carbon transport, *Mar. Chem.*, 59(1-2), 17–34, doi:10.1016/S0304-4203(97)00069-8, 1997.







Wommack, K.E. and Colwell, R.R.: Virioplankton: viruses in aquatic ecosystems, *Microbiol. Mol. Biol. Rev.*, 64, 69–114, 2000.

Worden, A. Z., Nolan, J., K., and Palenik, B.: Assessing the dynamics and ecology of marine picophytoplankton: The importance of the eukaryotic component. *Limnol. Oceanogr.*, 49, 168-179, doi:10.4319/lo.2004.49.1.0168, 2004.

Zuur, A. F., Ieno, E. N. and Smith, G. M.: *Analysing Ecological Data*, Springer New York, doi: 10.1007/978-0-387-45972-1, 2007.

1 **Table 1.** $f\text{CO}_2$ concentrations (μatm) averaged over the duration of the experiment
 2 (following CO_2 addition) and subsequent classification as low, intermediate or high.
 3 Mesocosms sampled for mortality assays are denoted by an asterisk. The symbols and
 4 colours are used throughout this manuscript and corresponding articles in this issue.

5
6

<i>Mesocosm</i>	<i>M1*</i>	<i>M5</i>	<i>M7</i>	<i>M6</i>	<i>M3*</i>	<i>M8</i>
<i>CO₂ Level</i>	<i>LOW</i>	<i>LOW</i>	<i>INTERMEDIATE</i>	<i>INTERMEDIATE</i>	<i>HIGH</i>	<i>HIGH</i>
<i>Mean $f\text{CO}_2$ (μatm) days 1-43</i>	<i>365</i>	<i>368</i>	<i>497</i>	<i>821</i>	<i>1007</i>	<i>1231</i>
<i>Symbol</i>						

7
8
9
10

1 **Table 2.** The fit (R^2) and significance (p -value) of linear regressions applied to assess the relationship
 2 between net growth rate and temporally averaged fCO_2 for the different microbial groups
 3 distinguished by flow cytometry. The results presented are for two periods distinguished from NMDS
 4 analysis; NMDS-based period 1 (days 3-13) and 2 (days 16-24). A significance level of $p \leq 0.05$ was
 5 taken and significant results are shown in bold.

6

<i>Phytoplankton Group</i>	<i>NMDS period 1 (days 3-13)</i>		<i>NMDS period 2 (days 16-24)</i>	
	<i>p</i>	<i>R²</i>	<i>p</i>	<i>R²</i>
<i>SYN</i>	0.10	0.53	0.05	0.63
<i>Pico-I</i>	0.01	0.80	0.05	0.64
<i>Pico-II</i>	0.52	0.11	0.10	0.52
<i>Pico-III</i>	0.04	0.67	<0.01	0.91
<i>Nano-I</i>	0.01	0.79	0.26	0.30
<i>Nano-II</i>	0.20	0.36	0.06	0.61
<i>HNA</i>	0.05	0.64	0.89	0.00
<i>LNA</i>	<0.01	0.95	0.02	0.76

7

8

9

10

1 **Table 3.** The fit (R^2) and significance (p -value) of linear regressions used to relate peak abundances
 2 and net growth rate with temporally averaged fCO_2 for the different microbial groups distinguished
 3 by flow cytometry during specific periods of interest. A significance level of $p \leq 0.05$ was taken and
 4 significant results are shown in bold.

5
6
7

	<i>Peak abundance</i>		<i>Net growth rate</i>	
	<i>p</i>	<i>R2</i>	<i>p</i>	<i>R2</i>
<i>SYN day 24</i>	0.01	0.80		
<i>Pico-I day 5</i>	0.01	0.81		
<i>Pico-I day 13</i>	<0.01	0.94		
<i>Pico-I day 21</i>	0.01	0.84		
<i>Pico-II day 17</i>	<0.01	0.93		
<i>Pico-III day 24</i>	<0.01	0.91		
<i>Nano-I day 17</i>	0.04	0.67		
<i>Pico-I days 1-5</i>			<0.01	0.90
<i>Pico-I days 5-9</i>			<0.01	0.89
<i>Pico-II days 12-17</i>			0.01	0.82

8
9
10
11
12
13
14
15
16
17

1 **Figure captions**

2

3 **Fig. 1. (a)** Time-series plot of depth-integrated (0.3–10 m) total phytoplankton abundance (< 20 μm)
4 and **(b)** total eukaryotic phytoplankton abundance for each mesocosm and the surrounding waters
5 (Baltic). Dotted lines indicate the end of Phase I and end of Phase II. Colours and symbols represent
6 the different mesocosms and are consistent throughout the manuscript. Mean $f\text{CO}_2$ during the
7 experiment (days 1-43) were: M1, 365 μatm ; M3, 1007 μatm ; M5, 368 μatm ; M6, 821 μatm ; M7,
8 497 μatm ; M8, 1231 μatm .

9

10 **Fig. 2.** Non-metric multidimensional scaling (NMDS) ordination plot of microbial community
11 development in each mesocosm and surrounding waters (Baltic) over the experimental period.
12 Phases are indicated by different open symbols. Days of experiment (DoE) when communities
13 separate (3,13,16 and 24) are indicated by different closed symbols. Phytoplankton groups are
14 denoted as: SYN (Syn), Pico-I (P-I), Pico-II (P-II), Pico-III (P-III), Nano-I (N-I), Nano-II (N-II), Low NA
15 prokaryotes (LNA) and High NA prokaryotes (HNA).

16

17

18 **Fig. 3.** Time-series plot of depth-integrated (0.3–10 m) abundances of **(a)** *Synechococcus* (SYN) **(b)**
19 picoeukaryotes I (Pico-I) **(c)** picoeukaryotes II (Pico-II) **(d)** picoeukaryotes III (Pico-III) **(e)**
20 nanoeukaryotes I (Nano-I) and **(f)** nanoeukaryotes II (Nano-II) distinguished by flow cytometric
21 analysis of the microbial community in each mesocosm and the surrounding waters (Baltic). Dotted
22 lines indicate the end of Phase I and end of Phase II, grey areas indicate NMDS-based periods 1 and 2
23 where net growth rates were analysed.

24

25

26 **Fig. 4.** Total mortality rates (i.e., grazing and lysis, solid bars) and gross growth rates (striped bars) d^{-1}
27 of the different phytoplankton groups in mesocosms M1 (blue) and M3 (red) on the day indicated:
28 **(a)** *Synechococcus* (SYN) **(b)** picoeukaryotes I (Pico-I) **(c)** picoeukaryotes II (Pico-II) **(d)** picoeukaryotes
29 III (Pico-III) **(e)** nanoeukaryotes I (Nano-I) and **(f)** nanoeukaryotes II (Nano-II). Significant ($p \leq 0.05$)
30 differences between mesocosms are indicated by an asterisk above the relevant bar (either total loss
31 or gross growth). A colored zero indicates that a rate of zero was measured in the mesocosm of the
32 corresponding colour and the absence of a bar, or zero indicates a failed experiment. Dotted lines
33 indicate the end of Phase I and end of Phase II.

34

35

36 **Fig. 5.** Time-series plot of the mean phytoplankton carbon biomass in high $f\text{CO}_2$ (M3,6,8; red) and low
37 $f\text{CO}_2$ (M1,5,7; blue) mesocosms of **(a)** Pico I and II combined and **(b)** SYN, Pico III, Nano I and II

1 combined. Error bars represent one standard deviation from the mean. Carbon biomass calculated
2 assuming a spherical diameter equivalent to the mean average cell diameters for each group and
3 conversion factors of 237 fg C μm^{-3} (Worden et al.2004) and 196.5 fg C μm^{-3} (Garrison et al. 2000) for
4 pico- and nano-sized plankton, respectively. Dotted lines indicate the end of Phase I and end of Phase
5 II.

6

7 **Fig. 6.** Time series plot of depth-integrated (0.3–10 m) abundances of **(a)** Total prokaryotes **(b)** High
8 fluorescent nucleic acid prokaryote population (HNA) **(c)** Low fluorescent nucleic acid prokaryote
9 population (LNA) and **(d)** Total virus. Dotted lines indicate the end of Phase I and end of Phase II, grey
10 areas indicate NMDS-based periods where net growth rates were analysed.

11

12 **Fig. 7.** Prokaryote mortality rates: **(a)** Total grazing (d^{-1}) and **(b)** viral lysis rates as % of prokaryote
13 standing stock, in mesocosms M1 (low $f\text{CO}_2$, blue) and M3 (high $f\text{CO}_2$, red). Grazing rates were
14 determined from fluorescently labelled prey, viral lysis rates from viral production assays. Error bars
15 represent one standard deviation of triplicate assays. Significant ($p \leq 0.05$) differences between
16 mesocosms are indicated by an asterisk. Dotted lines indicate the end of Phase I.

17

18 **Fig. 8.** Correlation between total carbon biomass ($\mu\text{mol L}^{-1}$) and total prokaryote abundance in low
19 $f\text{CO}_2$ mesocosms (M1, 5 and 7; blue) and high $f\text{CO}_2$ mesocosms (M3,6, 8; red) throughout the
20 experiment (days -2 to 39).

21

22

23

24

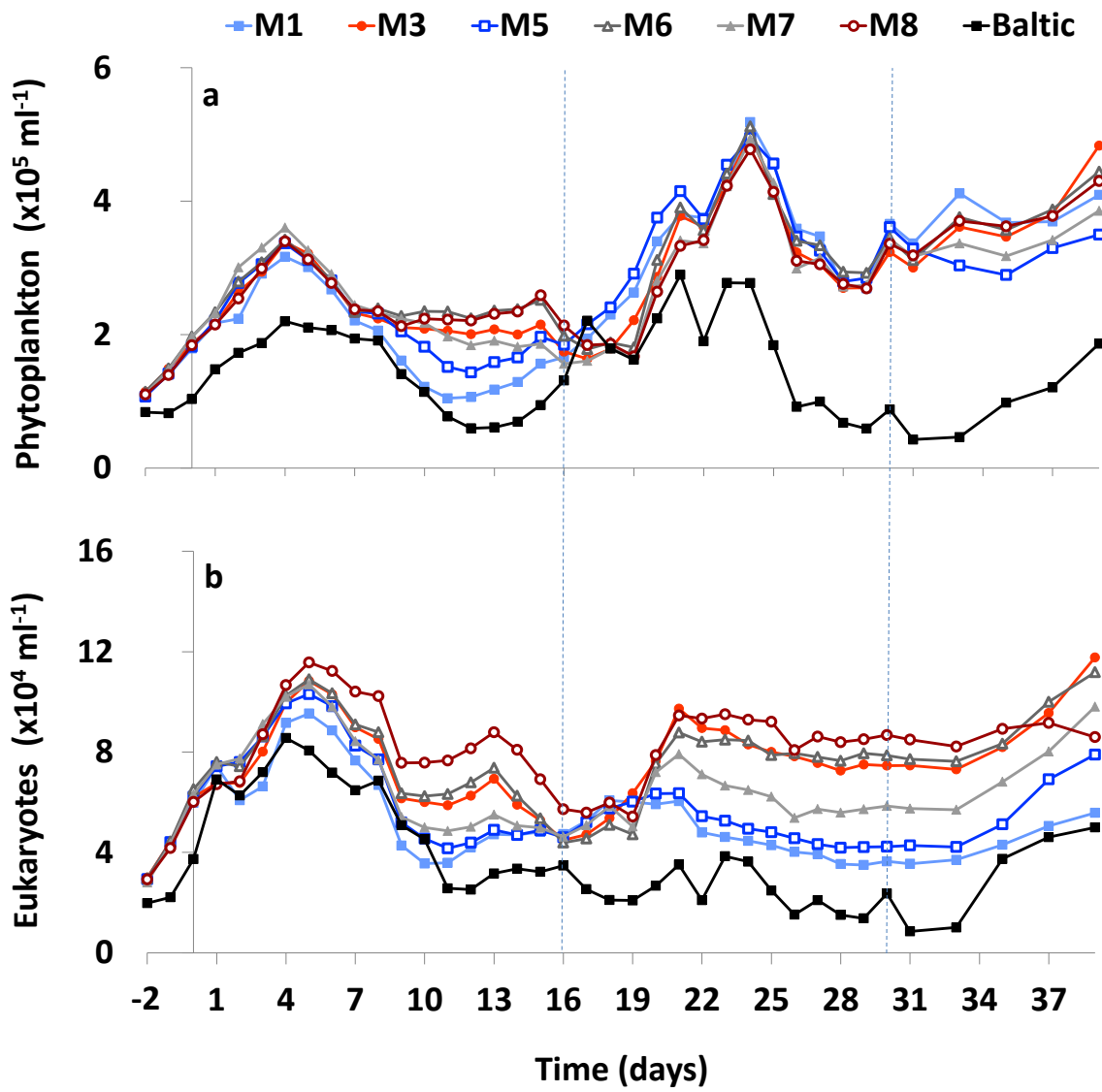


Figure 1.

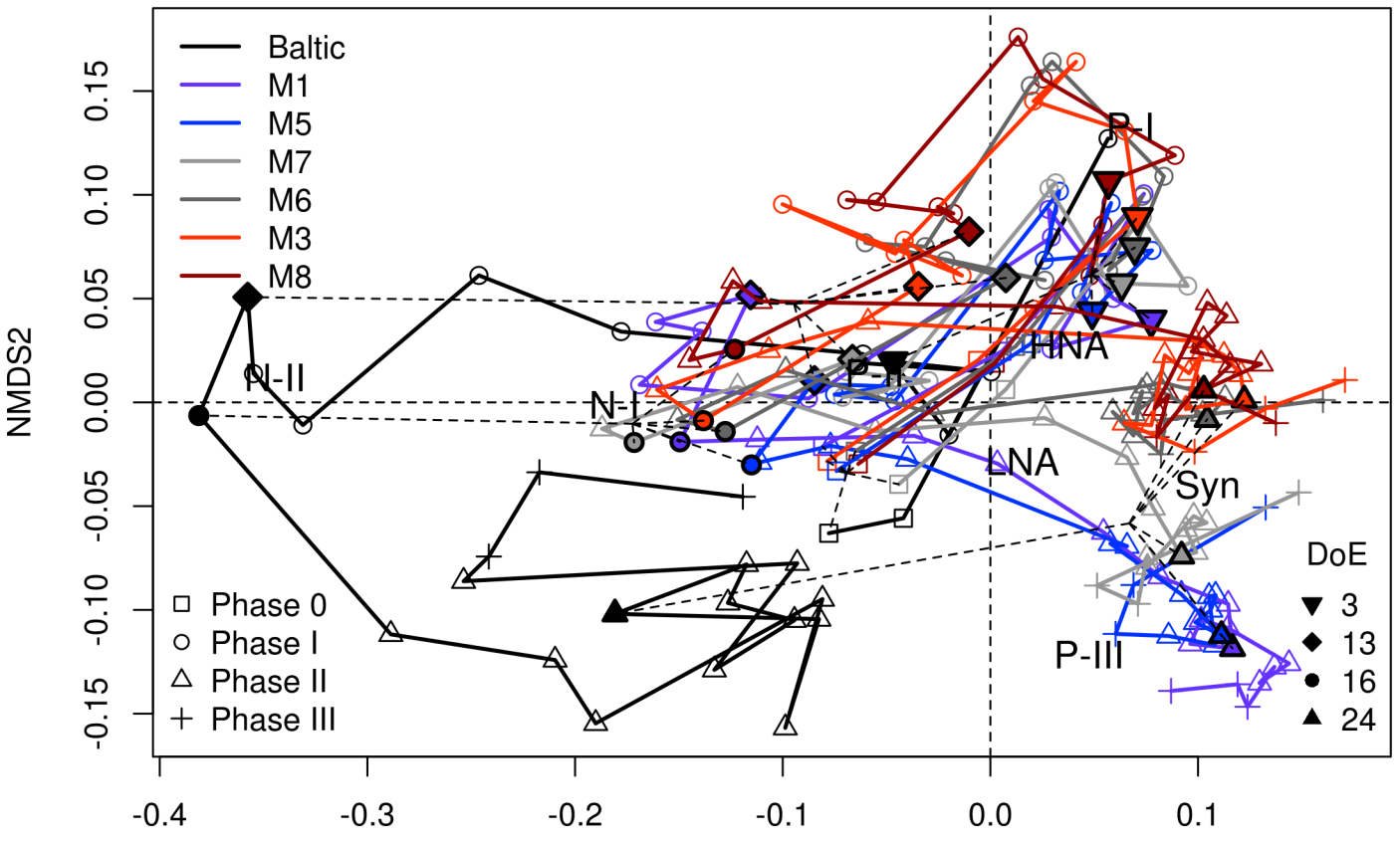


Figure 2.

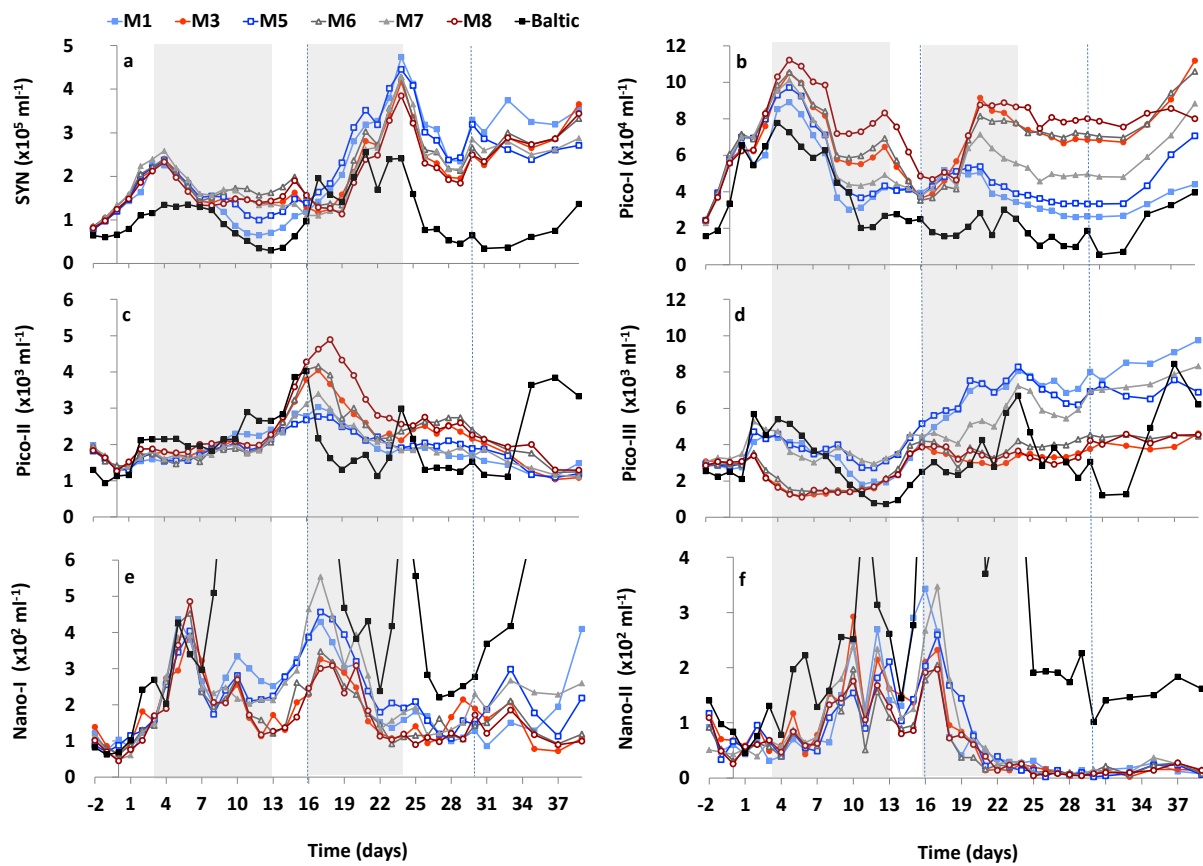


Figure 3.

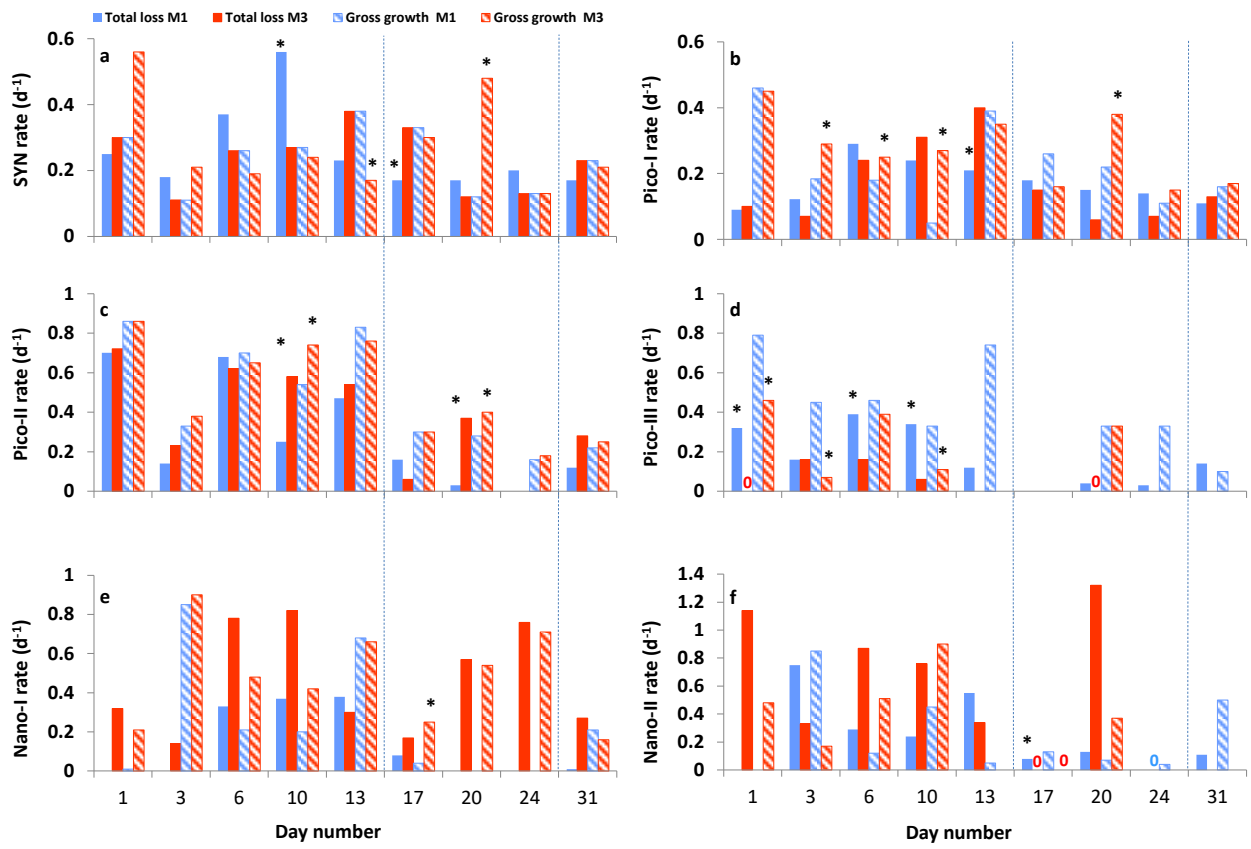


Figure 4.

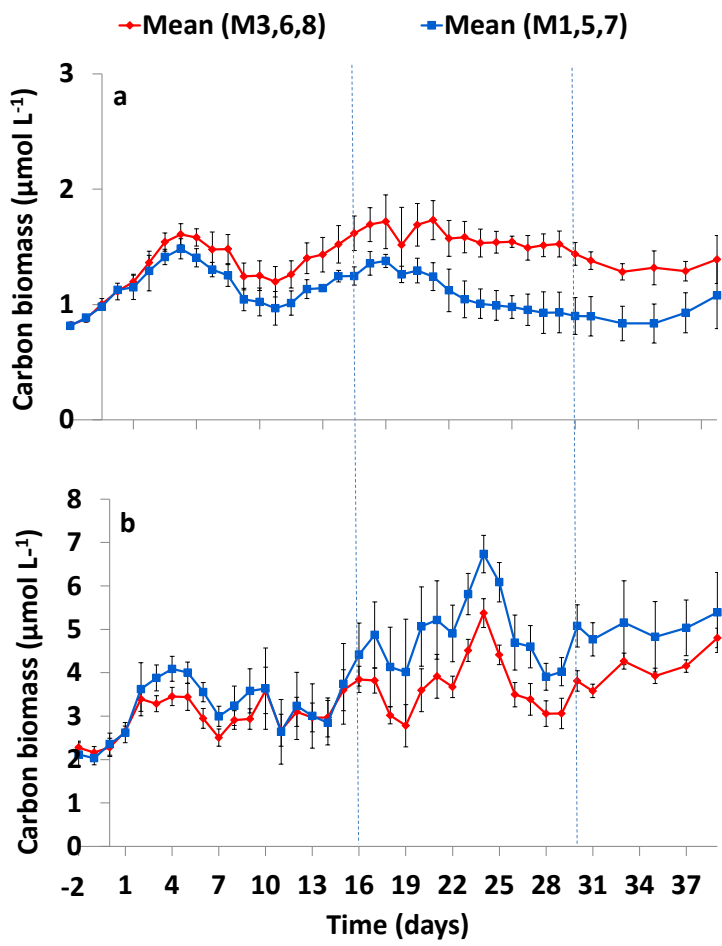


Figure 5.

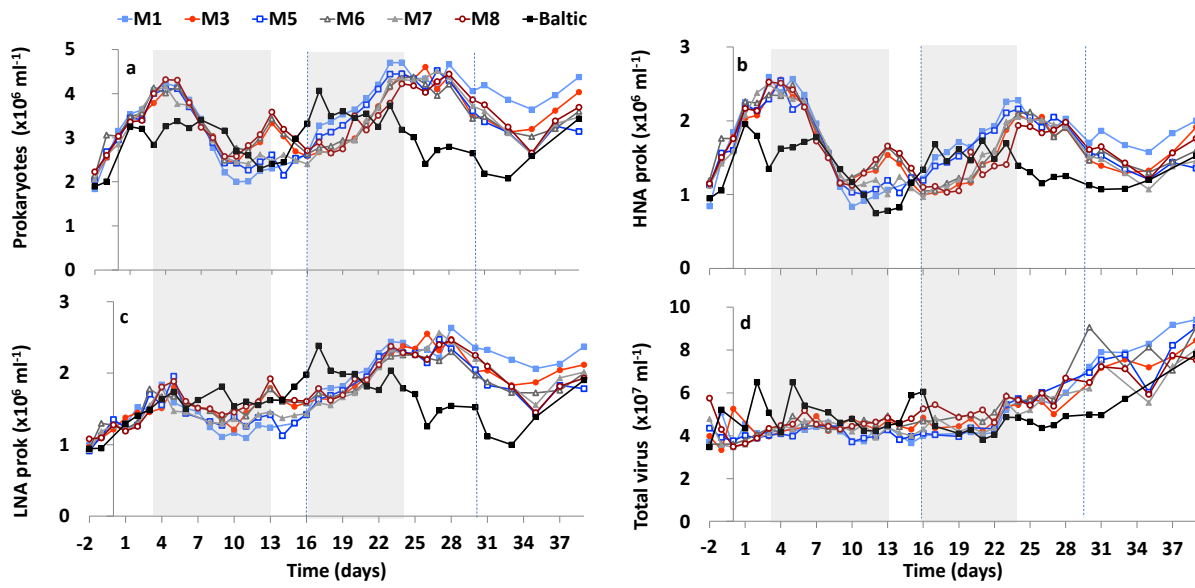


Figure 6.

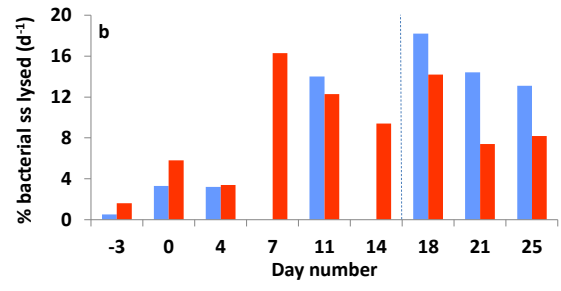
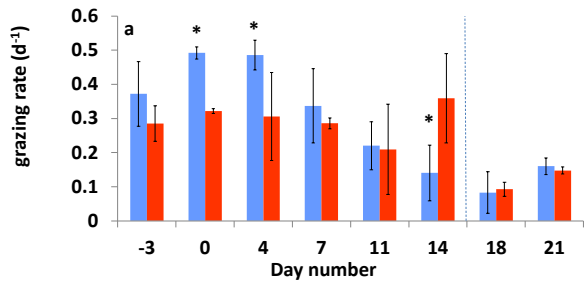


Figure 7.

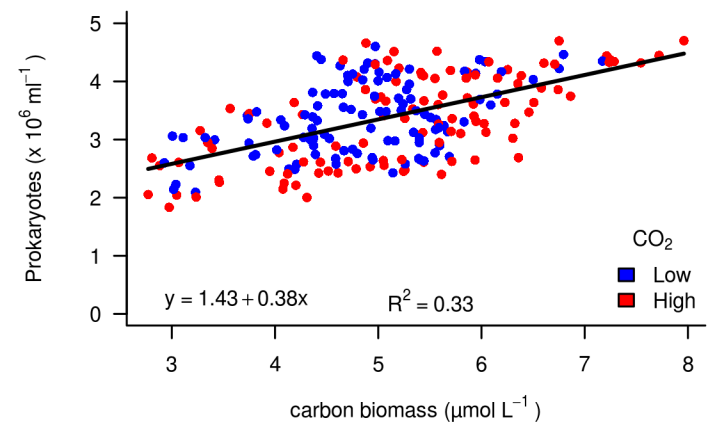


Figure 8.